



**HAL**  
open science

## Fluid properties and dynamics along the seismogenic plate interface

Hugues Raimbourg, Vincent Famin, Giulia Palazzin, Mathieu Mayoux,  
Laurent Jolivet, Claire Ramboz, Asuka Yamaguchi

► **To cite this version:**

Hugues Raimbourg, Vincent Famin, Giulia Palazzin, Mathieu Mayoux, Laurent Jolivet, et al.. Fluid properties and dynamics along the seismogenic plate interface. *Geosphere*, 2018, 14 (2), pp.469-491. 10.1130/GES01504.1 . insu-01717256

**HAL Id: insu-01717256**

**<https://insu.hal.science/insu-01717256v1>**

Submitted on 26 Feb 2018

**HAL** is a multi-disciplinary open access archive for the deposit and dissemination of scientific research documents, whether they are published or not. The documents may come from teaching and research institutions in France or abroad, or from public or private research centers.

L'archive ouverte pluridisciplinaire **HAL**, est destinée au dépôt et à la diffusion de documents scientifiques de niveau recherche, publiés ou non, émanant des établissements d'enseignement et de recherche français ou étrangers, des laboratoires publics ou privés.



Distributed under a Creative Commons Attribution - NonCommercial 4.0 International License

GEOSPHERE, v. 14, no. 2

doi:10.1130/GES01504.1

13 figures; 2 tables; 1 supplemental file

## CORRESPONDENCE:

hugues.raimbou@univ-orleans.fr

CITATION: Raimbourg, H., Famin, V., Palazzin, G., Mayoux, M., Jolivet, L., Ramboz, C., and Yamaguchi, A., 2018, Fluid properties and dynamics along the seismogenic plate interface: *Geosphere*, v. 14, no. 2, doi:10.1130/GES01504.1.

Science Editor: Shanaka de Silva  
Guest Associate Editor: Philippe Agard

Received 23 January 2017  
Revision received 21 September 2017  
Accepted 19 December 2017



This paper is published under the terms of the CC-BY-NC license.

© 2018 The Authors

# Fluid properties and dynamics along the seismogenic plate interface

Hugues Raimbourg<sup>1,2,3</sup>, Vincent Famin<sup>4</sup>, Giulia Palazzin<sup>1,2,3</sup>, Mathieu Mayoux<sup>1,2,3</sup>, Laurent Jolivet<sup>1,2,3</sup>, Claire Ramboz<sup>1,2,3</sup>, and Asuka Yamaguchi<sup>5</sup>

<sup>1</sup>Université d'Orléans, Institut des Sciences de la Terre D'Orléans, UMR 7327, 45071 Orléans, France

<sup>2</sup>Centre National de la Recherche Scientifique, Institut des Sciences de la Terre D'Orléans, UMR 7327, 45071 Orléans, France

<sup>3</sup>Bureau de Recherches Géologiques et Minières, Institut des Sciences de la Terre D'Orléans, UMR 7327, BP 36009, 45060 Orléans, France

<sup>4</sup>Laboratoire Géosciences Réunion, Université de La Réunion, Institut de Physique du Globe de Paris, Sorbonne Paris Cité, UMR 7154, Centre National de la Recherche Scientifique, Saint-Denis, La Réunion, France

<sup>5</sup>Department of Ocean Floor Geoscience, Atmosphere and Ocean Research Institute, The University of Tokyo 5-1-5 Kashiwanoha, Kashiwa, Chiba 277-8564, Japan

## ABSTRACT

Fossil structures, such as exhumed accretionary prisms, are the only direct recorders of the fluids wetting the plate interface near the base of the seismogenic zone. By studying exhumed accretionary prisms, it is thus possible to determine the physicochemical properties of fluids and the geometry and dynamics of their circulation. We considered here two transects encompassing the brittle-plastic transition (BPT) zone, in the Franco-Italian Alps and the Shimanto Belt in Japan, and compared our data with a broader set of examples from the literature. On quartz that grew synkinematically at peak burial conditions, we inferred fluid properties indirectly from quartz trace-element concentrations (using cathodoluminescence [CL] imaging) and directly from fluid-inclusion composition and P-p-T properties (using Raman and microthermometry). At ~250 °C, quartz grew principally through fracturing and two types of quartz, a CL-brown and a CL-blue, precipitated alternately. At ~350 °C, where plastic deformation and recrystallization is pervasive, only a single, homogeneously CL-brown quartz is present. The salinity of the fluid in the inclusions shallower than the BPT is consistently of the order or lower than seawater, while salinities are very scattered deeper than the BPT and often exceed seawater salinity. The gas dissolved in the fluid is predominantly CH<sub>4</sub> shallower than the BPT, and either CH<sub>4</sub> or CO<sub>2</sub> deeper than the BPT, depending on the nature of the host rock and in particular on the proportion of carbonates. Cathodoluminescence properties, salinity, and nature of the gas all point to a closed-system behavior in rocks deeper than the BPT. In contrast, shallower than the BPT (i.e., at seismogenic depths), textures revealed by CL-imaging evidence the episodic influx of an external fluid, leading to the crystallization of CL-blue quartz. The scale of the circulation leading to the generation of the CL-blue quartz, or its relationship with the seismic cycle, is still unclear. Besides, the fluid pressure recorded in the abundant water-rich fluid inclusions is systematically much lower than the corresponding lithostatic pressure, irrespective of the depth domain considered. For inclusions trapped at large depth, the low fluid pressure recorded in the inclusions reflects post-entrapment reequilibration. For inclusions trapped at shallower conditions, typically at seismogenic depths, the low fluid pressure may as well be the result of large fluid pressure drop after earthquakes.

## INTRODUCTION

### Fluid Fluxes along the Plate Interface

The flux of fluid along the plate interface and in overlying accretionary prism has been extensively studied in the shallow domain (i.e., less than a few km depth) of subduction zones in the framework of deep-sea drilling campaigns. Based on direct observations or measurements of venting (e.g., Henry et al., 1992) or hydrological models (e.g., Bekins and Dreiss, 1992), the general scheme of shallow fluid circulation is that water dragged passively down in pores of buried sediments is expelled by compaction and flows upward along permeable horizons such as faults and a master décollement (Kastner et al., 1991; Le Pichon et al., 1993; Saffer and Tobin, 2011). This source of water is restricted to a few kilometers of depth, as the pore volume fraction diminishes along with compaction, and is replaced by water produced by dehydration reactions, involving for example clay minerals, abundant in buried sediments (Saffer and Tobin, 2011).

Models of “deep” fluid flow (i.e., deeper than ~10 km depth) are much more unclear, because the relevant physical properties (permeability, porosity and fluid production) are not well constrained in modern margins. For example, physical properties are to a large extent derived from measurements of P-wave velocities ( $V_p$ ), using relationships that are well calibrated for a large porosity (Erickson and Jarrard, 1998; Raimbourg et al., 2011; Kitajima and Saffer, 2012). Below 20%–30% porosity, the empirical relationships to convert  $V_p$  into porosity and then to relate porosity to permeability (Neuzil, 1994) are much more uncertain. Furthermore, as temperature increases, rock physical properties depend not only on porosity but also on chemical processes such as cementation or mineral reactions, in relationship with solid deformation (e.g., Tsuji et al., 2006).

Models of deep fluid flow rely therefore mostly on geochemical studies in fossil subduction zones, focusing on isotopic reequilibration or elemental transfers in metamorphic rocks. These studies help discriminate whether the chemical exchanges are restricted to compositionally homogeneous domains (e.g., a tectonic slice of metapelites or serpentines) or whether chemical exchanges occur over larger scales, across different domains. The different units

from the Franciscan Complex span the T range 100–350 °C, corresponding to the seismogenic zone (Sadofsky and Bebout, 2001). Most carbonate veins formed in these units are host-rock buffered in terms of oxygen and carbon isotopes, with in some cases the contribution of the advection of an external fluid with a higher  $\delta^{18}\text{O}$  (Sadofsky and Bebout, 2004). Such local control is in agreement with the  $\delta^{18}\text{O}$  in the quartz veins from the Shimanto Belt (Lewis and Byrne, 2003; Raimbourg et al., 2015), irrespective of the CL color of the quartz, or from the Alps (Mullis et al., 1994). In Kodiak, similar host-rock buffering of quartz in veins is described in Vrolijk (1987a, 1987b) but for quartz veins in tectonic mélanges, where  $\delta^{18}\text{O}$  is higher than in veins from coherent units. Another contrasting example is provided by the Otago Schists of New Zealand, where the  $\delta^{18}\text{O}$  signature of quartz veins points to the reequilibration with the pore-fluid reservoir rather than host-rock buffering (Fagereng and Harris, 2014). Therefore, in terms of isotopes, the general regime is a buffering of fluid and vein isotopic composition by host rock, even if several cases point to a mixing with a fluid external to the system, possibly flowing from the depth and enriched in heavier  $^{18}\text{O}$ .

At larger depths, metasediments in the Franciscan Complex or the Schistes Lustrés in the Alps, buried down respectively to ~30 km and ~45 km, mostly retain their concentrations in fluid-mobile elements, attesting to closed-system behavior (Busigny et al., 2003; Sadofsky and Bebout, 2003; Scambelluri and Philippot, 2004; Bebout, 2007; Bebout et al., 2013). Similarly, serpentines buried in the Alps retain their mobile elements and  $\delta^{18}\text{O}$  for T lower than the antigorite break down (~600–700 °C) (Scambelluri and Philippot, 2004; Scambelluri et al., 2004). These two cases correspond to low-T gradients prevailing in most subduction zones, so that limited mobility of elements seems to be the general case in material subducted to high-pressure conditions, even if more open-system behavior may occur under higher geothermal gradients (e.g., the Catalina Schists in California; Bebout, 2007).

In contrast to this general picture of closed-system behavior given by geochemical analyses, there is a systematic decrease in the water content of subducted rocks as a result of progressive metamorphism. Because we consider the release of water at depths larger than a few km, we focus hereafter on water bound to minerals rather than water in rock pores. Incoming material, composed of sediments, extrusives forming the uppermost horizon of the oceanic crust, dikes, and gabbros carry on average 7 wt% (Plank and Langmuir, 1998), ~3–6 wt%, ~2 wt%, and 1 wt%, respectively (for a 20–80 Ma oceanic lithosphere; Jarrard, 2003) of mineral-bound  $\text{H}_2\text{O}$ , although these quantities may vary significantly depending, for example, on the nature of subducting sediments or the slab hydration through faulting and influx of water at the outer rise (Ranero et al., 2003). The oceanic crust is the largest  $\text{H}_2\text{O}$  reservoir to be subducted (Bebout, 1995; van Keken et al., 2011). Dehydration reactions occur as a result of prograde metamorphism, at different depths depending on the layer considered. In sediments, dehydration reactions start at low temperature, of the order of 50 °C, with reactions such as opal  $\rightarrow$  quartz or smectite  $\rightarrow$  illite (Moore and Saffer, 2001; Saffer and Tobin, 2011). The latter reaction is the principal source of water, and it is completed at T of ~150 °C. As a result,

the water left in metasediments of the Santa Catalina Schists and Franciscan Complex, buried to conditions below 300 °C and 1 GPa, has already decreased to ~3 wt% (Sadofsky and Bebout, 2003). In the crust, dehydration reactions are deeper and mostly localized at ~80 km depth, except in the warmest slabs, where they can occur at shallower depths (Van Keken et al., 2011). As a result, by ~80 km depth, a large fraction of the water initially present has escaped the crust and the sediments of the slab.

There is therefore a decoupling between the large volumes of fluid flowing from and through the subducting slab and the limited transport of elements with the fluid. For this reason, many geochemical tracers seem unable to track the fluid circulation and its geometry, as for example oxygen isotopes that are host-rock buffered while microstructures point to a complex interplay of two fluids during vein precipitation (Raimbourg et al., 2015). Only domains of focused fluid flow, such as the highly sheared rocks of the subduction channel (e.g., Vannucchi et al., 2010), may be able to record isotopically the flow of exotic fluid without complete host-rock buffer.

Additional information on fluid flow is provided by microstructures, in particular veins, which are witnesses of fluid circulation at depth. In fossil subduction zones, the large concentration of veins in rocks interpreted as belonging to a paleoplate interface provides evidence of vigorous and localized fluid circulations (Byrne and Fisher, 1990; Vannucchi et al., 2010; Yamaguchi et al., 2012). The interpretation of such geological structures in terms of fluid circulation is nevertheless difficult. Certain models plead in favor of large-scale advective flow (Ferry and Dipple, 1991; Breeding and Ague, 2002), but other evidence, such as the ubiquitous and pervasive occurrence of dissolution microstructures in accretionary prisms (Kawabata et al., 2007; Raimbourg et al., 2009), or mass-balance calculations on the required amount of fluid flow to fill the veins with quartz (Fisher and Brantley, 1992; Fisher et al., 1995), point rather to local sources for vein-forming elements. Furthermore, the possible link between fluid flow and deformation, in particular earthquakes, suggested by crack-seal textures in veins (Fisher and Brantley, 1992, 2014; Fagereng et al., 2011), remains hypothetical.

## Fluid Pressure along the Plate Interface

Associated with the question of fluid circulation, fluid pressure is another key issue in subduction zones. Because it is potentially a major control on plate boundary strength and seismic and/or aseismic character, many studies have focused on the amplitude of the overpressures of fluid in and around the plate interface (defined as the excess with respect to the hydrostatic fluid pressure gradient). At depths of a few km, seismic reflection profiles (Shibley et al., 1990; Tobin and Saffer, 2009) or hydrological models (Shi and Wang, 1985; Saffer and Bekins, 1998) suggest, in many subduction margins, the existence of near-lithostatic fluid pressure in underthrust sediments and in the overlying décollement (see review by Saffer and Tobin, 2011), resulting from the compaction of high-porosity sediments. At larger depths, down to typically ~30–40 km, overall large overpressures of fluid within the upper part of the

subducting slab are inferred from high  $V_p/V_s$  ratio in several subduction zones such as New Zealand (Eberhart-Phillips et al., 2005), Costa Rica (Audet and Schwartz, 2013), Chile (Moreno et al., 2014), or southwestern Japan (Kato et al., 2010). In addition, some of these seismological studies (Audet and Schwartz, 2013; Moreno et al., 2014) indicate a correspondence between the amplitude of overpressure and the seismic-aseismic character of the interface, suggesting some causal relationship.

The geological record corresponding to these geophysical observations of high fluid pressure in modern margins, consists first of the abundance of extension veins in exhumed mélanges interpreted as paleoplate interface zones, such as in the Apennines (Meneghini et al., 2007; Vannucchi et al., 2010), Alaska (Fisher and Brantley, 2014), or the Franciscan Complex (Meneghini and Moore, 2007). Mode I fracture requires fluid pressure to be larger than  $\sigma_3$ , hence close to lithostatic pressure, because differential stress is presumably small in subduction zones (Lamb, 2006; Hasegawa et al., 2012; Duarte et al., 2015). These extension veins confirm therefore the average high pore-fluid pressure along the plate interface but provide limited insights into the space and time distribution of such a pressure field.

The study of fluid inclusions is another potentially powerful tool to estimate the fluid pressure at depth and to derive the amplitude of fluid overpressure from its comparison with rock pressure. This objective faces two distinct obstacles in the shallow and large depth domain. At shallow depth, where low temperature (T) prevails ( $T < \sim 300$  °C), corresponding to the seismogenic zone, there is hardly any reliable geobarometer to derive rock pressure, hence the record of fluid inclusion is in most cases the only available information about pressure. A good example is the Shimanto Belt, where a wealth of fluid-inclusion studies is available to derive the fluid pressure (Sakaguchi, 1996; Sakaguchi, 1999b; Lewis and Byrne, 2003; Matsumura et al., 2003; Okamoto et al., 2014) but where the corresponding rock peak pressure conditions are not well constrained (Underwood et al., 1993), preventing an estimate of the degree of fluid overpressuring. At large pressure, for example in the blueschist- and eclogite-facies fields, the fluid inclusions record systematically low fluid pressure with respect to the pressure conditions derived from mineral assemblages (Küster and Stöckert, 1997; Agard et al., 2000). The pressure record in the fluid inclusions is interpreted as reflecting not the actual pressure during entrapment, but posterior reequilibration at lower pressure during uplift. In summary, both at low and high pressure, there is a limited geological record of concomitant fluid and rock pressure, to be compared with geophysical observations.

Still, fluid inclusions may provide useful insights into the time variations in fluid pressure, despite limitation with regard to the assessment of the absolute value of fluid overpressure. Variations in the density of methane trapped in fluid inclusions from synkinematic quartz veins were reported in the Kodiak accretionary complex in Alaska (Vrolijk, 1987a, 1987b) and in the Shimanto Belt (Raimbourg et al., 2017) and were interpreted as reflecting cycles of fluid pressure. In this interpretation, the cyclic drop in fluid pressure results from episodes of fracturing and connection of a fault network, enabling the fluid to

escape to shallower domains. It is nevertheless not clear whether the triggering of fracturing is due to the fluid itself (through a fluid pressure rise resulting from tectonic loading or chemical reactions) or results from damage during large earthquakes.

The objective of this work is to provide examples of the geological record of the composition and pressure of the deep fluid, as well as its flow patterns, using quartz veins and the fluid inclusions they contain. The two case studies, in the Alps and in the Shimanto Belt in Japan, encompass the depth range that includes the transition from macroscopically brittle behavior to deformation controlled by crystal plasticity (BPT), which is often correlated to the transition from seismic to aseismic behavior of the plate interface (Hyndman et al., 1997; Oleskevich et al., 1999). We have focused on synkinematic quartz veins and studied the evolution with burial depth and temperature of (1) microstructures and vein generations (with optical microscopy and cathodoluminescence) and (2) nature and pressure of the fluid trapped in inclusions (with Raman spectroscopy and microthermometry). These observations reveal a sharp contrast in fluid circulation between the seismogenic plate interface and the deeper aseismic domain. In addition, a compilation of our data with the literature shows that the record of fluid pressure in fluid inclusions is systematically lower than the corresponding conditions of lithostatic pressure along the subduction plane.

## CHOICE OF THE SAMPLES AND METHODS OF ANALYSIS

### Sampling Areas

To study the evolution with depth of the fluid along the plate interface, we have already studied in detail the example of the Shimanto Belt in Japan (Raimbourg et al., 2014b; Raimbourg et al., 2015; Palazzini et al., 2016), and we describe hereafter the principal results (Fig. 1). The Western Alps provide another well-studied example of subducted sediments (Fig. 2). In both settings, we have selected quartz veins belonging to two units with a contrast in metamorphic temperature, one “high-T” (~350 °C) unit and one “low-T” unit (~250 °C) (as defined by Raman spectrum of organic matter, see below), so as to study the downdip limit of the seismogenic zone and the transition from brittle to plastic deformation of quartz. The position of all samples and outcrops described hereafter can be found in Supplemental Table S1<sup>1</sup>.

### Shimanto Samples

The Shimanto accretionary complex, exposed on-land along the Honshu, Kyushu, and Shikoku islands in Japan (Fig. 1), is interpreted as an ancient accretionary prism (Taira et al., 1980; Taira et al., 1988). The whole complex, trending parallel to the modern trench axis of the Nankai Trough, is composed of a stack of units with a general dip toward the N or NW, with a younging trend toward the SE. These units are constituted of either coherent sedimentary units or tectonic mélanges.

Unit	Outcrop	Sample	Longitude	Latitude
Foliated Morotsuka		HN 44	131.37826	32.51452
		HN52-bis	131.24250	32.41610
		HN 61	131.85588	32.72024
		HN 63	131.47757	32.60295
		HN145	131.55827	32.61372
		HN196	131.31005	32.49335
		HN285	131.23915	32.42005
		203C	131.10535	32.42470
Hyuga Tectonic mélange		HN 51	131.24250	32.41610
		HN 54	131.73098	32.59126
		HN 64	131.46297	32.59442
		HN 65	131.40357	32.54517
		HN 68	131.39923	32.54939
		HN 75	131.24460	32.41619
		HN 77	131.24460	32.41619
		HN 85	131.31481	32.42867
		HN 91	131.24250	32.41610
		HN 93	131.58203	32.60445
		HN 94	131.57563	32.60837
		HN200	131.31412	32.42883
		HN299	131.27900	32.40332
		202M	131.27817	32.41513
Schistes lustrés	2B	6.86482	44.97524	
		10B	Haute vallée de l'Ubaye (6.89062)	(44.60916)
		6.96795	44.60493	
Figure 3D				
Fylsch à Helminthoides		FH2	6.72594	44.52633
		F6H2	6.72594	44.52633
		FH4	6.76392	44.52242
		FH7-2	6.82747	44.33592
		FH12	6.74108	44.50108
		FH21b	6.74458	44.51531
		FH22	6.70521	44.53585
		FH103B	6.81894	44.33214
		FH114	6.65147	44.55842
		Figure 3B	6.72594	44.52633

<sup>1</sup>Supplemental Table S1. Location of all samples and outcrops used in this work. Please visit <http://doi.org/10.1130/GES01504.S1> or the full-text article on [www.gsapubs.org](http://www.gsapubs.org) to view Supplemental Table S1.

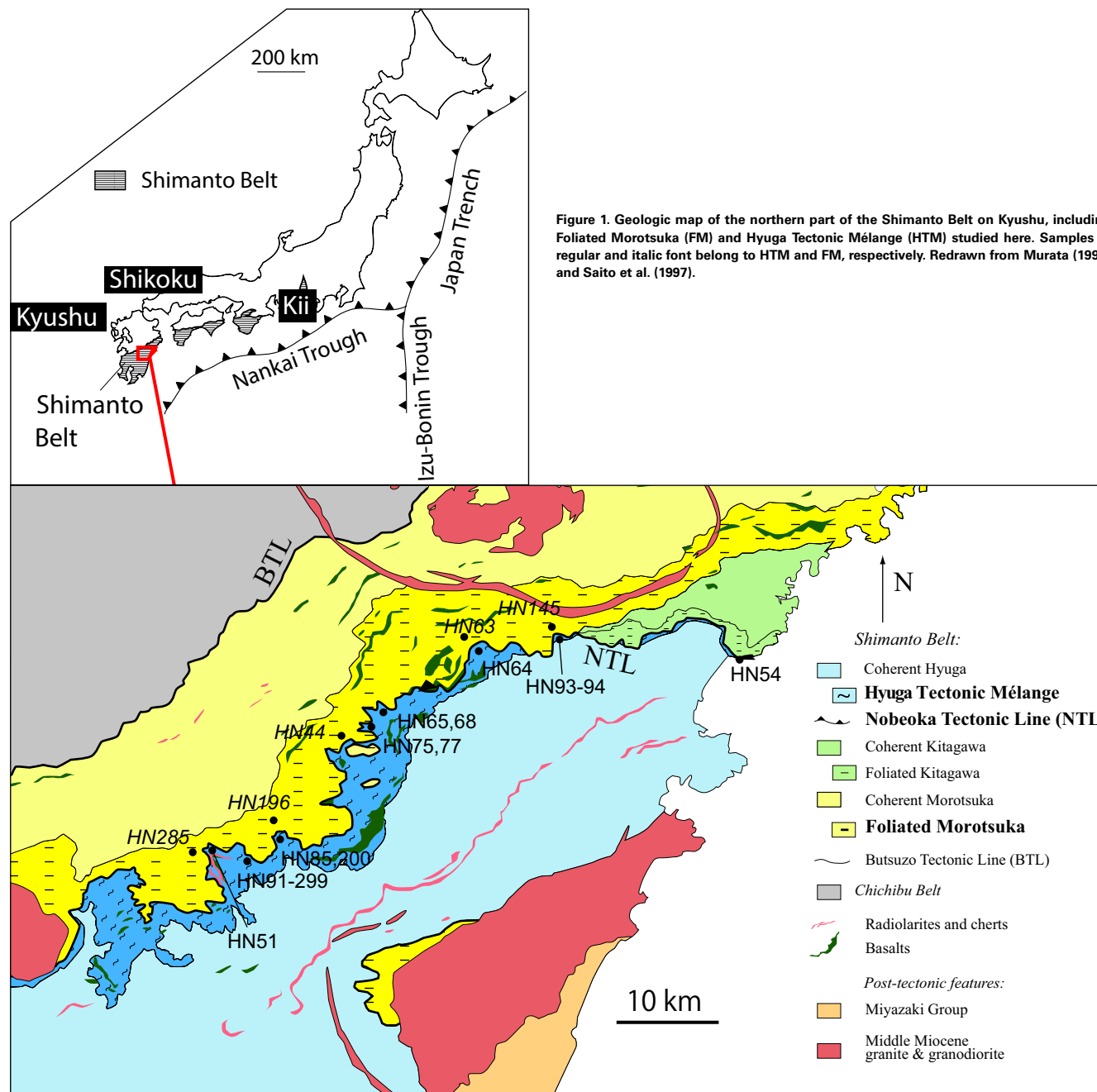
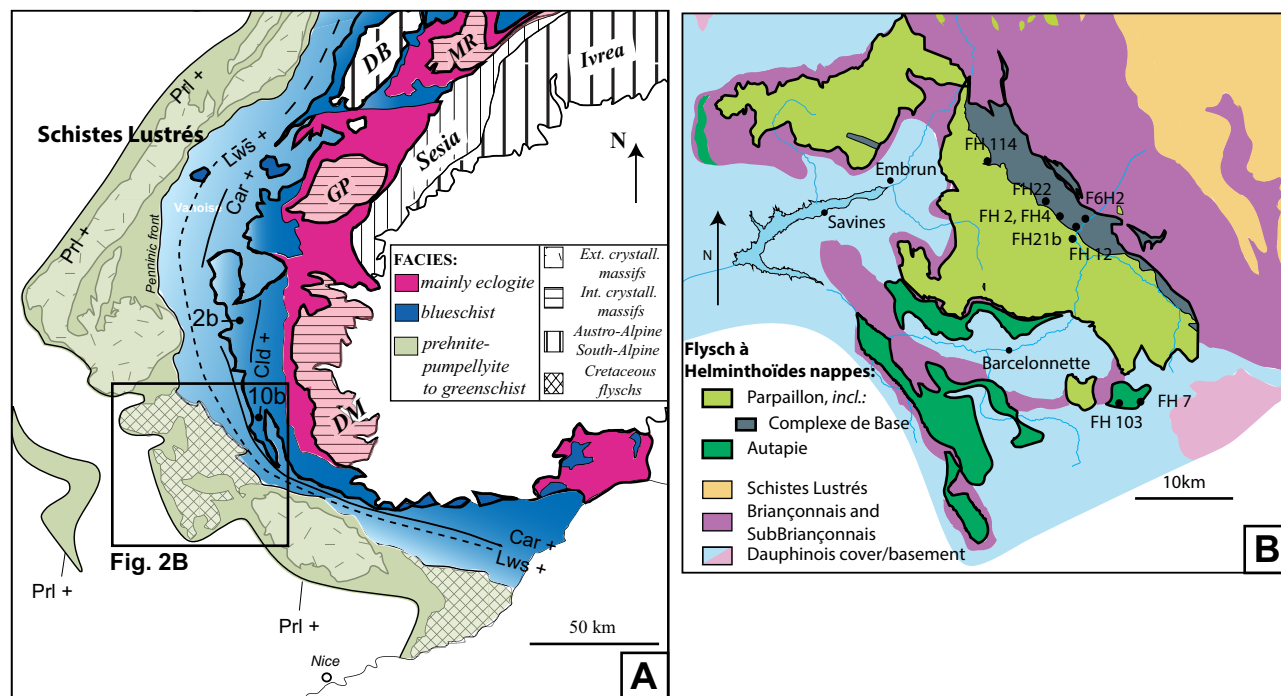


Figure 2. (A) Large-scale geologic map of the Alps, showing the position of the two units studied here: SL—Schistes Lustrés and FH—Flysch à Helminthoïdes, along with the metamorphic gradient across the Belt, apparent in the distribution of index metamorphic minerals (from Saliot et al., 1980; Goffé and Chopin, 1986). Mineral abbreviations: Car—carpholite; Cld—chloritoid; Lws—lawsonite; Prl—pyrophyllite. Geologic unit abbreviations: MR—Monte Rose; GP—Gran Paradiso; DM—Dora Maira; DB—Dent Blanche. (B) Close-up view of the Flysch à Helminthoïdes with the studied samples (from Kerckhove et al., 1980). SL and FH limits are underlined by thick lines in (A) and (B), respectively. Both sections modified from Agard and Lemoine (2003).



Our study focuses on the northern portion of the Belt on Kyushu, namely the basal layer of the Morotsuka Group, i.e., the Foliated Morotsuka (FM) (Raimbourg et al., 2014a) and the upper part of the Hyuga Group, known as the Hyuga Tectonic Mélange (HTM). The two units are juxtaposed by the Nobeoka Tectonic Line (NTL), a large-scale, low-dipping thrust fault (Saito et al., 1996; Murata, 1997).

The HTM constitutes the best example of plate interface deformation: it consists of strongly sheared sandstone and quartz boudins in a pelitic matrix, with a direction of movement to the SE consistent with the coeval subduction of the Pacific plate below Japan (Faccenna et al., 2012). Synkinematic quartz veins formed within rigid blocks, such as sandstones, as extension veins perpendicular to lineation, or as shear veins at low angle to the foliation (Fig. 3A; see also Palazzin et al., 2016). The temperature of deformation is  $\sim 245 \pm 30$  °C, as can be determined from Raman spectrum of organic matter (Palazzin et al., 2016), and the quartz microstructures recorded mostly pressure solution, with a minor contribution of plastic deformation.

The FM formation, of pelitic composition, constitutes the “high-T” end member of this study, as metamorphic T is  $\sim 345 \pm 30$  °C (Palazzin et al., 2016). Kinematics of the deformation are mostly subhorizontal flattening, resulting in folding and transposing of earlier-stage quartz veins (Fig. 3C). Quartz in veins

is mostly recrystallized and develops accordingly a crystallographic preferred orientation, with a concentration of quartz c-axes along Z kinematic direction (Palazzin et al., 2016). In tectonic reconstructions of the margin evolution, this deformation event occurred in the vicinity of the plate interface as a result of the collapse of the accretionary prism in the Paleogene (Raimbourg et al., 2014a).

### Alps Samples

The nappe du Parpaillon, within the Flysch à Helminthoïdes unit (FH), is constituted of  $\sim 1000$ -m-thick series of calcareous turbidites overlying a level of dark pelites containing thin sandstone beds (“Complexe de Base” [CB]) (Kerckhove, 1963; Kerckhove et al., 2005). Rare fossils give an upper Cretaceous age (Kerckhove, 1963), contemporaneous with the upper levels of the Schistes Lustrés (SL). Similarly to the SL, the FH nappe is interpreted as associated to the Liguro-Piemontese oceanic domain (Kerckhove, 1963; Caron et al., 1981). This paleogeographic position involves large displacement of the Parpaillon Nappe upon emplacement, and the CB constitutes the associated niveau de décollement (Kerckhove et al., 2005). The deformation of the Nappe comprises two phases of folding (Merle and Brun, 1981; Merle, 1982) achieved at low-grade conditions, at most greenschist-facies conditions (Bousquet et al., 2012).

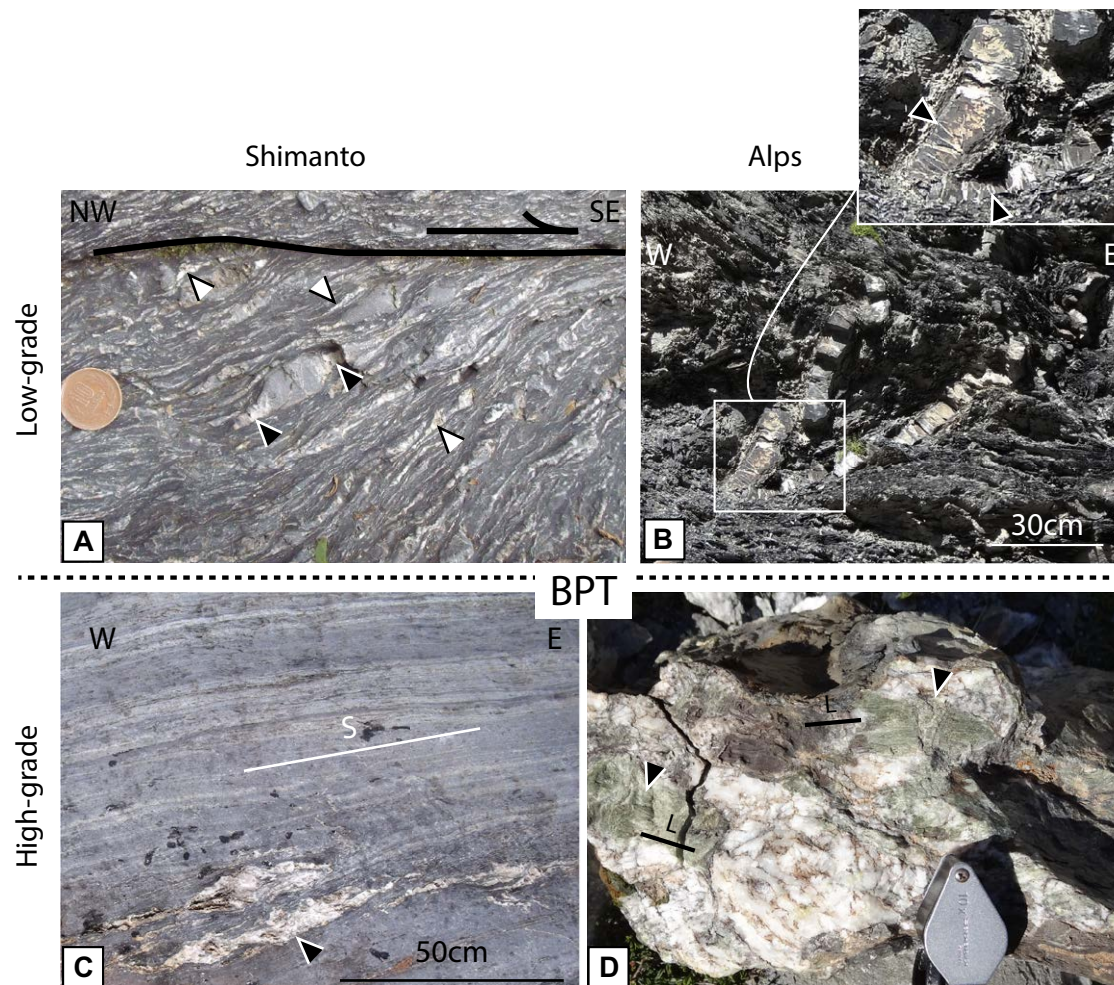


Figure 3. (A) Block-in-matrix structure of the Hyuga Tectonic Mélange. Sandstone blocks have boudinaged tails (black triangles) composed mostly of quartz veins perpendicular to stretching direction. In addition, quartz veins also constitute blocks elongated parallel to stretching direction (white triangle). Stretching is the result of shearing on a top-to-the-SE shear zone on top of the picture (outcrop 202M). (B) Sandstone bed folded isoclinally, showing predating quartz veins (triangles) rotated in the fold hinge, from the Flysch à Helminthoïdes. (C) Quartz vein (triangles) flattened and transposed parallel to the schistosity S in Foliated Morotsuka (outcrop 203C). (D) Large quartz vein preserved from plastic deformation, incorporating patches of carpholite fibers elongated in different directions of lineation L, from the Schistes Lustrés. BPT—brittle-plastic transition.

The early stage of deformation is recorded by isoclinal folding, with an axis orientated NE-SW and transport direction toward the NW (Merle and Brun, 1981; Merle, 1982). In the CB, this deformation is apparent through the isoclinal folding of thin turbidites beds, which develop a schistosity as axial planes of folds. These folded beds are in addition cut by numerous quartz veins, oriented approximately perpendicular to bedding. These veins constitute an early-stage deformation feature as they are refolded by isoclinal folds (Fig. 3B). All the early-stage deformation features recorded in the CB (isoclinal folding, extension veins, and schistosity) may be interpreted as associated with the displacement along the basal décollement and the layer-parallel

shearing, the régime that prevails in underplated units in accretionary prisms (Byrne and Fisher, 1990; Vannucchi et al., 2010; Fisher and Brantley, 2014). So even if the evolution of the FH during the subduction of the Liguro-Piemontese Ocean is relatively ill constrained, we tentatively consider its basal unit and the early deformation it records as an analogue of underplated units in subduction complexes.

The Schistes Lustrés Complex is a large portion of the cover of the Ligurian oceanic basement, including ophiolitic slivers of various sizes (Lemoine et al., 1986; Michard et al., 1996; Stampfli and Marchant, 1997) and subducted down to blueschist- and eclogite-facies conditions during the Alpine orogenesis

(Caby et al., 1978; Saliot et al., 1980; Goffé and Chopin, 1986; Agard et al., 2000). In the studied area (Fig. 2), the SL are composed of metapelites affected by increasing metamorphic conditions from west to east (Chopin and Schreyer, 1983; Beyssac et al., 2002). In the westernmost area, the metapelites contain the HP index mineral magnesio-carpholite, principally present with quartz in veins (Fig. 3D), formed at peak metamorphic conditions of ~350–380 °C and ~15 kbars (Agard et al., 2000). The close association, with quartz veins, of tiny needles of carpholite and primary fluid inclusions, was taken as evidence of the formation of these fluid inclusions at peak conditions, although they suffered some reequilibration during retrograde evolution (Agard et al., 2000). The kinematics of the tectonic stage associated with the carpholite-bearing veins (D1 stage by Agard et al., 2001) is unclear, as it is in most places obscured by top-to-the-east D2 stage related to exhumation.

### Comparison of the Selected Samples

The four cases studied are meant as representative of deformation of sediments along or near the subduction plane at different depths and temperatures. There are nevertheless large contrasts in two different respects between the Alpine and the Japanese example.

The first difference is the metamorphic gradient during burial. Conditions for the Shimanto Belt, derived in the highest-grade units, are of the order of 3–5 kbars and 300–350 °C (Toriumi and Teruya, 1988; Palazzin et al., 2016), i.e., 15–30 °C/km, and hence belong to a relatively high metamorphic gradient. In contrast, the SL metamorphism is associated with a very cold gradient, because roughly similar temperatures but much higher pressures are reported for the western domain of the SL (~350–380 °C and ~15 kbars [Agard et al., 2000]; i.e., ~6 °C/km).

The second difference is the abundance of carbonates. The Alpine units (SL and FH) contain a large proportion of carbonates (Kerckhove, 1969; Caron, 1977). In contrast, the sedimentary units constituting the Shimanto Belt contain a relatively low abundance of carbonates (Taira et al., 1988). This general feature applies to the Hyuga mélange, where recent X-ray diffraction (XRD) semiquantitative analyses of lithology show proportion of calcite less than 10% and in most cases less than a few % (Fukuchi et al., 2014).

### Analytical Techniques

Samples similar to Figure 3 were processed into thin sections (for optical microscopy, Raman spectroscopy, cathodoluminescence, and electronic and ion microprobe) and thick sections (for microthermometry on fluid inclusions). Thin sections are ~30 µm thick and diamond polished on their upper surface. Thick sections are ~100–200 µm thick and diamond polished on both surfaces. Thin and thick sections were all cut perpendicular to the foliation and, whenever observed, parallel to the stretching lineation.

### Raman Spectra of Organic Matter

Raman spectroscopy of carbonaceous material (RSCM) thermometry is based on the quantitative estimate of the degree of structural transformation of carbonaceous material (CM) (Beyssac et al., 2002; Lahfid et al., 2010). Because of the irreversible character of graphitization, Raman spectrum of CM can be correlated with peak-T conditions (noted  $T_{\max}$  hereafter).

Raman spectra were obtained using a Renishaw InVIA Reflex microspectrometer (Institut des Sciences de la Terre d'Orléans [ISTO]–Bureau de Recherches Géologiques et Minières [BRGM]). A laser (514 nm) was focused on the sample by a DM2500 Leica microscope equipped with a  $\times 100$  objective. Instrument control and Raman measurements were performed with the software package Renishaw Wire 4.0. Acquisition time was generally over 30 s, and spectra were accumulated once or twice. To avoid defects on the CM related to thin-section preparation, analyses were all performed below the surface of the section by focusing the laser beam beneath a transparent crystal (i.e., dominantly quartz and occasionally calcite or albite). The laser beam power at sample surface was set to ~0.5 mW.

To interpret Raman spectra, we used the procedure of Lahfid et al. (2010) adapted to the low-grade metamorphic rocks considered here. This decomposition of spectra is based on five peaks, forming a defect band centered ~1350  $\text{cm}^{-1}$  (peaks D1, D3, and D4) and a graphite band centered ~1580–1600  $\text{cm}^{-1}$  (peaks D2 and G).  $T_{\max}$  can then be estimated, with an uncertainty of  $\pm 25$  °C, as  $RA1 = 0.0008 T_{\max} + 0.3758$ , where RA1 is the ratio of the peak areas defined as  $RA1 = (D1 + D4) / (D1 + D2 + D3 + D4 + G)$ . Note that the thermometer is calibrated for the range 200–320 °C, but for the sake of discussion, we used the correlation  $RA1 - T_{\max}$  for all samples where the decomposition in five peaks appropriately described the whole Raman spectrum, i.e., in the range 170–370 °C (see Table 1). To allow the comparison of RSCM analyses between the high-grade units of the Shimanto Belt and the SL, which were already analyzed by Beyssac et al. (2002), we also carried out the decomposition of Raman spectra in three peaks, calibrated for the temperature range 330–650 °C by the authors.

### Cathodoluminescence on Quartz

Samples were placed in a vacuum chamber at an argon pressure of  $\sim 60 \times 10^{-3}$  mbar. They were irradiated by a cold cathode source electron gun provided by Optique Electronique OPEA (France). Standard tension-current beam conditions were maintained at ~13–15 kV and 90–110 µA, respectively. The angle between the gun axis and horizontal was 18°. The chamber was placed on a simplified optical mount designed to minimize light absorption on the beam pathway. The optical stage was equipped with a Retiga 2000R 1394a cooled camera (captor size 1 inch, resolution 1600  $\times$  1200 pixel<sup>2</sup>, square pixel size 7.4 µm). The luminescence of quartz being quite low, acquisition time was fixed to ~10 s. Whenever present, the strong luminescence of carbonate veins prevented the analysis of quartz.



TABLE 1. PALEOTEMPERATURES ESTIMATED FROM RAMAN SPECTRA OF ORGANIC MATTER

Area	Unit	Sample	Longitude	Latitude	Number of analyses	RA1 = (D1 + D4)/ (D1 + D2 + D3 + D4 + G)	R2 = D1/ (G + D1 + D2)	Mean temperature (°C)	Temperature (standard deviation)	Average T (°C) (Lahfid et al., 2010)	Average T (°C) (Beysac et al., 2002)
Shimanto	Foliated Morotsuka	HN 44	131.3782566	32.5145217	9	0.663		356	21	351	327
		HN52-bis	131.2425042	32.4161024	10	0.663	0.742	311	13		
		HN 61	131.8558849	32.7202371	10	0.656	0.663	357	23		
		HN 63	131.4775705	32.6029473	9	0.652	0.680	346	8		
	Hyuga Tectonic mélange	HN 54	131.7309834	32.5912574	10	0.540	0.736	348	6	241	
		HN 64	131.4629731	32.5944187	9	0.565		338	6		
		HN 65	131.4035731	32.5451741	10	0.567		240	6		
		HN 68	131.3992347	32.5493934	10	0.587		264	22		
		HN 75	131.2446024	32.4161858	10	0.570		244	11		
		HN 77	131.2446024	32.4161858	10	0.585		261	27		
		HN 85	131.3148107	32.4286718	10	0.569		242	11		
		HN 91	131.2425042	32.4161024	10	0.561		233	8		
		HN 93	131.5820251	32.6044481	10	0.570		244	16		
		HN 94	131.5756283	32.6083713	10	0.563		235	13		
Alps	Schistes Lustrés	SL1			10 to 15		0.70	330		347	
		SL2			10 to 15		0.67	343			
		SL3			10 to 15		0.67	343			
		SL4			10 to 15		0.62	365			
		SL5			10 to 15		0.64	356			
	Flysch à Helminthoïdes	F6H2	6.725944	44.526333	11	0.610		292	26	268	
		FH4	6.763917	44.522417	10	0.585		261	14		
		FH7-2	6.827472	44.335917	10	0.595		273	17		
		FH12	6.741083	44.501083	9	0.582		258	19		
		FH103B	6.818944	44.332139	11	0.599		278	13		
		FH114	6.651470	44.558420	10	0.571		244	13		

Note: Paleotemperatures estimated using either Beysac et al. (2002) (italic font) or Lahfid et al. (2010) (plain font) procedure for high-grade (Foliated Morotsuka and Schistes Lustrés) and low-grade material (Hyuga Tectonic mélange and Flysch à Helminthoïdes) in the Shimanto Belt and in the Alps. To check the compatibility of the two procedures, we applied both methods on Foliated Morotsuka, with comparable results. Schistes Lustrés data from Beysac et al. (2002).

### Raman Spectra of Fluid Inclusions

Raman spectroscopy was carried out using a WITec Alpha500 RA system with a green laser ( $\lambda = 532$  nm, Nd:YAG frequency doubled laser) at the Centre de Biophysique Moléculaire, Orléans, France. The laser is connected to the system via an optical fiber and is focused on the surface using an optical microscope  $\times 100$  objective Nikon E Plan. In this configuration, the laser spot diameter is  $\sim 720$  nm. The laser power was set at 8 mW at the sample surface. Finally, two different gratings were used in order to obtain a spectral range of  $\sim 4000$   $\text{cm}^{-1}$  with a resolution of  $\sim 3$   $\text{cm}^{-1}$  or a spectral range of  $\sim 1300$   $\text{cm}^{-1}$  with a resolution of  $\sim 1$   $\text{cm}^{-1}$ .

### Microthermometry

**Apparatus and uncertainties.** Fluid-inclusion microthermometric measurements were carried out using the THMS-600 Linkam heating-cooling stage at ISTO (Orléans, France). Further details on apparatus and measurement conditions can be found in Raimbourg et al. (2014b). The temperature accuracy for these measurements is  $\pm 1$  °C, over the whole temperature range of investigation, from  $-120$  to  $+300$  °C. The range of temperatures  $\sim 0$  °C, relevant for ice-melting temperature of aqueous inclusions, was calibrated by using synthetic inclusions of pure water (freezing point at 0 °C) and water + CO<sub>2</sub> inclusions (melting point of CO<sub>2</sub> at  $-56.6$  °C), according to the procedure detailed in El

Mekki-Azouzi (2010). Measurements of ice-melting temperature, repeated over several sessions, on the same reference sample containing synthetic, pure-water inclusions, yielded differences of the order of 0.2 °C. In addition, measurements on synthetic, pure-water inclusions, over different reference quartz samples of various thicknesses (200–600 µm) and shapes, yielded differences as large as 0.6 °C between the samples. Because the rock slabs containing our natural fluid inclusions have various shapes and thicknesses, we estimate therefore the uncertainty of freezing stage measurement of ice-melting temperatures as ~0.8 °C.

**Choice of the fluid inclusions.** Fluid inclusions have a variable abundance, from rare and scattered in optically clear quartz grains to a dense network of fluid inclusions in cloudy quartz. Fluid inclusions typically range from a few up to 5 µm in diameter and they are two-phased at ambient temperature. Shapes range from elliptical to very irregular. We focused here on primary fluid inclusions, i.e., considering fluid inclusions with (1) a regular shape and (2) either isolated in the quartz crystal or at least not connected, spatially or in terms of elongation axis, with trails of secondary fluid inclusions. In addition, we focused on inclusions distributed only in domains of homogeneous CL color, to enable a clear correspondence between fluid properties and CL colors.

For the chosen fluid inclusions, we could observe and measure ice-melting temperature  $T_{mi}$  (where the last crystal of ice melts into the liquid),  $T_{mcl}$  (where the last crystal of gas hydrate melts into the liquid), and homogenization temperature  $T_h$  (where the bubble of gas vanishes by dissolution into the liquid). Temperatures  $T_h$  were easily assessed, because gas bubbles are agitated by Brownian motion. In contrast, the crystals of ice or gas hydrate could not be directly observed. Final melting of these crystals can only be inferred from a movement of the gas bubbles. In most fluid inclusions, when the last crystal melted, the gas bubble either (1) moved to a new position of equilibrium in the inclusion (and was then immobile upon temperature increase) or (2) appeared in the inclusion, since it was not visible at lower  $T$ .

## RESULTS

### Quartz Deformation Microstructures

The comparison of HTM and FM provides a good illustration of the onset of quartz plastic deformation as a result of  $T$  increase (Fig. 4). In HTM, quartz veins parallel to schistosity are mostly composed of large quartz grains slightly (Figs. 4A and 4B) to strongly (Fig. 4C) elongated parallel to the lineation. These megacrystals of quartz contain systematically a very large number of fluid inclusions. Some of these fluid inclusions align in planes perpendicular to the stretching direction, corresponding to healed extension microfractures (black triangle in Fig. 4C). Incipient recrystallization is apparent in fine-grained domains on the rims of megacrystals, with a large decrease in fluid-inclusion abundance (white triangle in Figs. 4B and 4C). In FM, recrystallization is pervasive: large inherited megacrystals, composed of patches of misoriented subgrains (Fig. 4D; D' and D'') alternate with fully recrystallized domains. Along with extensive recrystallization, the average fluid-inclusion abundance is much decreased. Additional in-

formation about deformation process is provided by electron backscatter diffraction (EBSD) analysis in Palazzin et al. (2016). Quartz crystallographic preferred orientation (CPO) in HTM, defined by a X-maximum, changes to a Z-maximum in FM. We interpreted this difference in CPO as the transition of fracturing and pressure-solution to plastic deformation-dominated deformation. The evolution from HTM to FM microstructures corresponds therefore to the BPT.

### Maximum Temperature of Deformation (by RSCM)

Paleotemperatures of the low-grade units HTM and FH, inferred from RSCM using Lahfid et al. (2010) procedure, are ~240 and ~270 °C ± 30 °C, respectively (Table 1). The estimated temperature of HTM is consistent with previous results based on vitrinite reflectance (Kondo et al., 2005) and illite crystallinity (Fukuchi et al., 2014). The analysis of the high-grade units, which stand on the edge of both procedures for low- (Lahfid et al., 2010) and high-grade (Beysac et al., 2002) material, can be carried out using both methods, yielding temperatures that differ only by ~20 °C. Using the Beysac et al. (2002) procedure gives paleotemperatures of ~330 and ~350 °C for the FM and the SL, respectively. There is therefore in both Japanese and Alpine cases a temperature gap of ~80 °C between high-grade and low-grade units, which is readily apparent on the general shape of organic matter spectra (Fig. 5).

### Quartz Generations (by Quartz Cathodoluminescence)

In low-grade units, quartz domains are composed of two distinct materials (Figs. 6A–6C): (1) CL-brown quartz, similar to the one present in high-grade domains (Figs. 6D and 6E) and (2) quartz characterized by a bright blue luminescence that vanishes upon exposition to the electron beam. The distribution of the two types of quartz, revealed by CL imaging, can be interpreted as fracture filling (Figs. 6A–6C) and growth rims (Fig. 6B). As the two reciprocal crosscutting (CL brown and blue crosscutting CL blue and brown) or growth (CL brown and blue overgrown on CL blue and brown) relationships can be observed, the two types of quartz precipitated alternately (see also Raimbourg et al., 2015). In general, CL-blue quartz forms larger veins (Fig. 6A), while CL-brown quartz fills much thinner veins (black triangles Fig. 6B), giving a “brecciated” aspect to domains initially formed of homogeneously CL-blue quartz (Fig. 6B). In contrast, in high-grade units, quartz is homogeneously constituted of a CL-brown material (Figs. 6D and 6E).

### Composition of the Gaseous Phase of Fluid Inclusions (by Raman)

Fluid inclusions present in the four units studied are two-phased at ambient  $T$ , with a bubble of gas embedded in liquid water. In HTM, prior Raman analyses have shown that the gas bubble is composed of methane (Raimbourg et al., 2014b). In the higher-grade FM, most of the quartz veins are plastically deformed and recrystallized (Palazzin et al., 2016) and contain a contrasted distribution of fluid inclusions. Inherited grains contain a relatively large amount

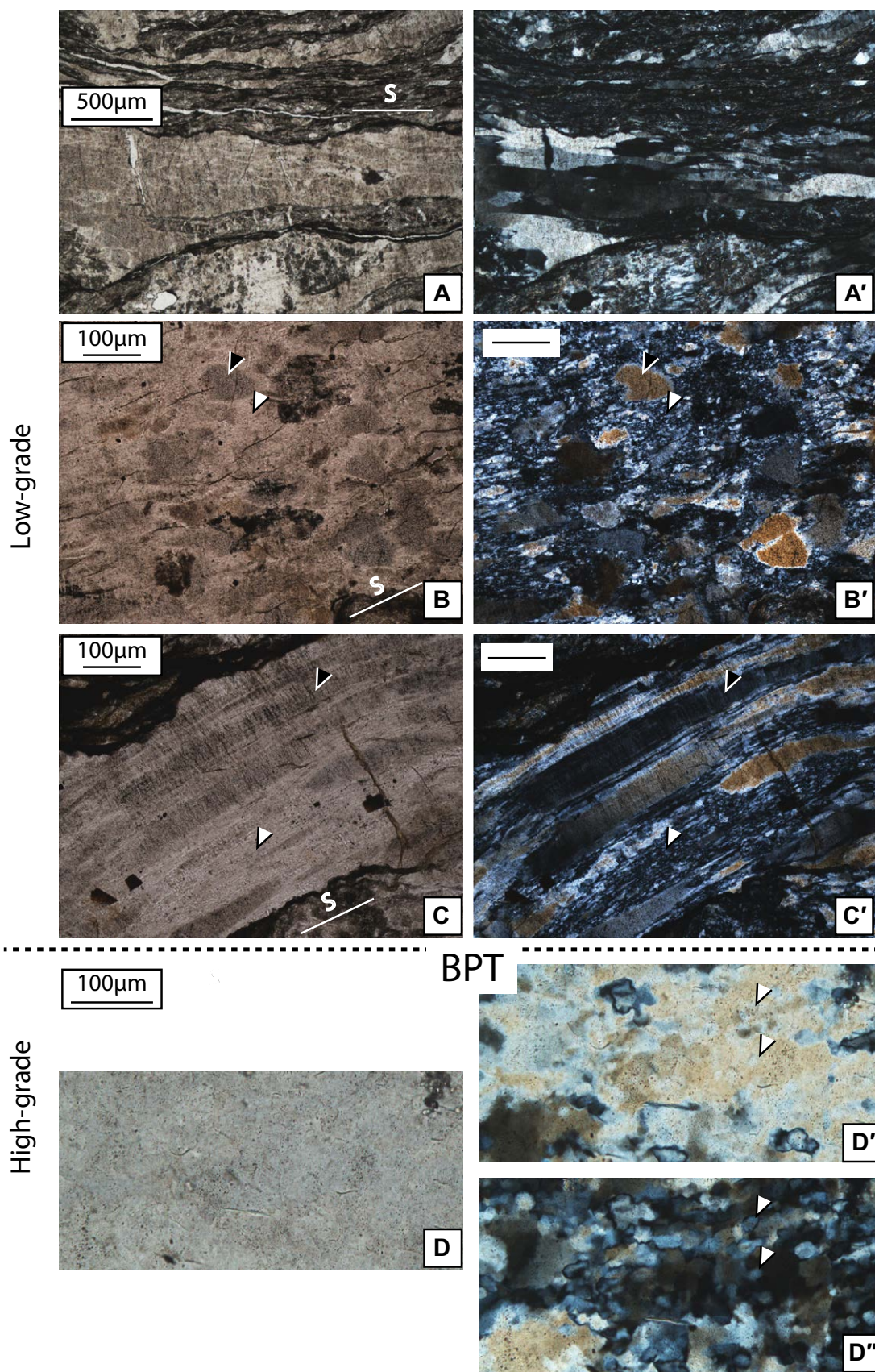


Figure 4. Quartz vein deformation microstructures across the temperature gradient, from Hyuga Tectonic Mélange (HTM) (A-A'-B-B'-C-C') to Foliated Morotsuka (FM) (D-D'-D''). (A-A') In HTM, most of the vein quartz is not recrystallized and contains a very high number of fluid inclusions. (B-B') Locally recrystallization occurs to form fine-grained aggregates (white arrow) with serrated grain boundaries, with a much lower fluid-inclusion abundance than in inherited grains (black arrow). (C-C') In strained domains, deformation results from microfracturing and pressure solution, as illustrated on a former microfracture, decorated with fluid-inclusion planes (black arrow), along with recrystallization (white arrows). (D-D'-D'') In Foliated Morotsuka (FM), at higher temperature, recrystallization is ubiquitous, and former large grains are replaced by misoriented subgrains (such as shown by the white arrows). S stands for the trace of the schistosity. Samples HN200 (A-A'), HN77 (B-B' and C-C'), and HN196 (D-D'-D''). Optical microphotographs without (A-B-C-D) and with (A'-B'-C'-D'-D'') crossed nicols. In D'', the orientation of polarizer and analyzer was rotated  $\sim 45^\circ$  with respect to D'. BPT—brittle-plastic transition.

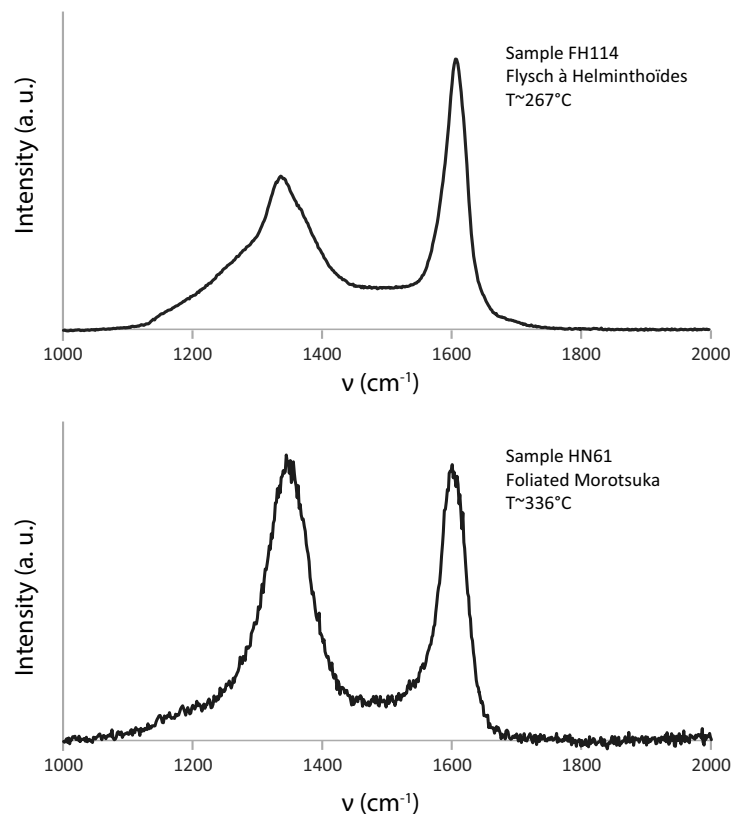


Figure 5. Typical spectra of organic matter particles disseminated in quartz, used for paleo-temperature estimates, in low-grade (top) and high-grade (bottom) units. a. u.—arbitrary units.

of fluid inclusions, while recrystallized and fine-grained domains contain a much lower abundance of fluid inclusions, which are in addition of a very small size, hence difficult to analyze. Irrespective of these microstructures, the gaseous bubble in all fluid inclusions is composed of methane (Fig. 7).

In the Alps, the fluid inclusions present with an extremely high abundance in the FH are composed of gaseous methane and water (Fig. 7). In contrast, the large quartz veins from the SL incorporating carpholite needles contain much fewer fluid inclusions. The gaseous bubble is composed there of  $\text{CO}_2$ , with no trace of methane.

In summary, the two low-grade units contain fluid inclusions made of a mixture of liquid water and gaseous methane. The high-grade units have a different gaseous phase in fluid inclusions. If methane fills the bubble in the FM in the Shimanto Belt, the gaseous phase in fluid inclusions from the SL is composed of  $\text{CO}_2$ .

## Fluid Physicochemical Properties (by Microthermometry on Fluid Inclusions)

In the Flysch à Helminthoïdes, the three microthermometric properties we could systematically observe—namely, last melting of ice, last melting of clathrate, and homogenization—are homogeneous across the four samples we analyzed (Fig. 8):  $T_{mi}$  ranges principally between  $-0.8$  and  $-2$  °C,  $T_{mcl}$  ranges between  $1$  and  $6$  °C, and  $T_h$  clusters between  $180$  and  $210$  °C (Table 2).

There is no systematic variation related to the CL color of the quartz hosting the fluid inclusions but for  $T_{mi}$ . In one sample (FH2), fluid inclusions in CL-blue quartz have a lower  $T_{mi}$ , hence a larger salinity, than those in CL-brown quartz; while in two other samples (FH22 and FH114A), there is no difference between the two types of quartz. In the fourth sample (FH21b), the number of data in the CL-brown quartz is too small for any conclusion to be drawn.

A synthetic, upper P-T isochore of these inclusions can be calculated using  $-2$  °C,  $5$  °C, and  $180$  °C, as  $T_{mir}$ ,  $T_{mcl}$ , and  $T_h$ , respectively, in the procedure in Raimbourg et al. (2014b). The associated concentration of methane is  $0.34$  mol  $\text{CH}_4/\text{kg H}_2\text{O}$  (Fig. 9). The intersection of this isochore with the rock paleo-temperature range by Raman occurs at  $\sim 2$  kbars.

## DISCUSSION

### Timing of Formation of the Fluid Inclusions

The timing of entrapment of the fluid in inclusions, with respect to host-rock evolution, is difficult to assess. In FH, we analyzed primary fluid inclusions whose entrapment is contemporaneous with host quartz growth, while in HTM (Raimbourg et al., 2015), we considered also secondary fluid inclusions when they could be unambiguously associated with fracture-filling quartz of a homogeneous CL color.

In the HTM case, both veins and microfractures filled by trails of fluid inclusions are systematically oriented perpendicular to the extension direction (Palazzin et al., 2016, their figures 6–8), and the quartz crystallographic fabrics itself is interpreted as reflecting growth by repeated events of fracturing and/or sealing. Fluid inclusions formed therefore principally during the main deformation event, which corresponds to peak burial conditions (Raimbourg et al., 2014a).

In the FH case, deformation kinematics during burial are obscured by later-stage deformation related to Alpine collision (Merle and Brun, 1981; Merle, 1982). One constraint on quartz veins formation is that they are an early-stage deformation feature, which predates folding, possibly during nappe transport. In addition, the geometry of the veins, i.e., perpendicular to bedding and concentrated in sandstone beds, is very similar to vein geometry in the Shimanto Belt (Raimbourg et al., 2015) or in Kodiak accretionary prism (Fisher and Byrne, 1987; Byrne and Fisher, 1990). In this last example, penetrative extension fracturing of sandstone beds in turbidite units is operative throughout burial. On the basis of deformation analysis, the record of fluid inclusions in both HTM and FH can be associated with burial or peak metamorphic conditions.

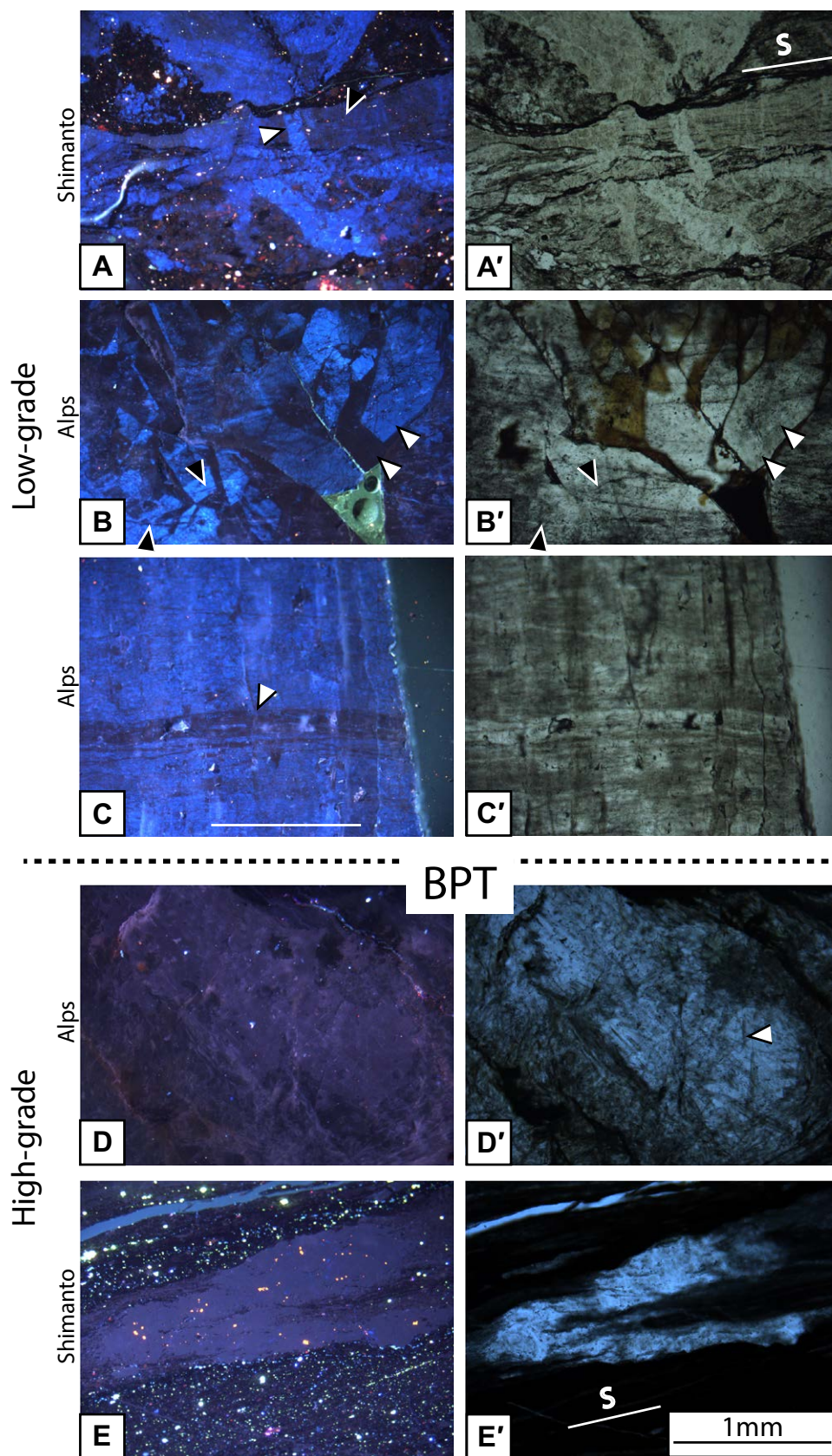
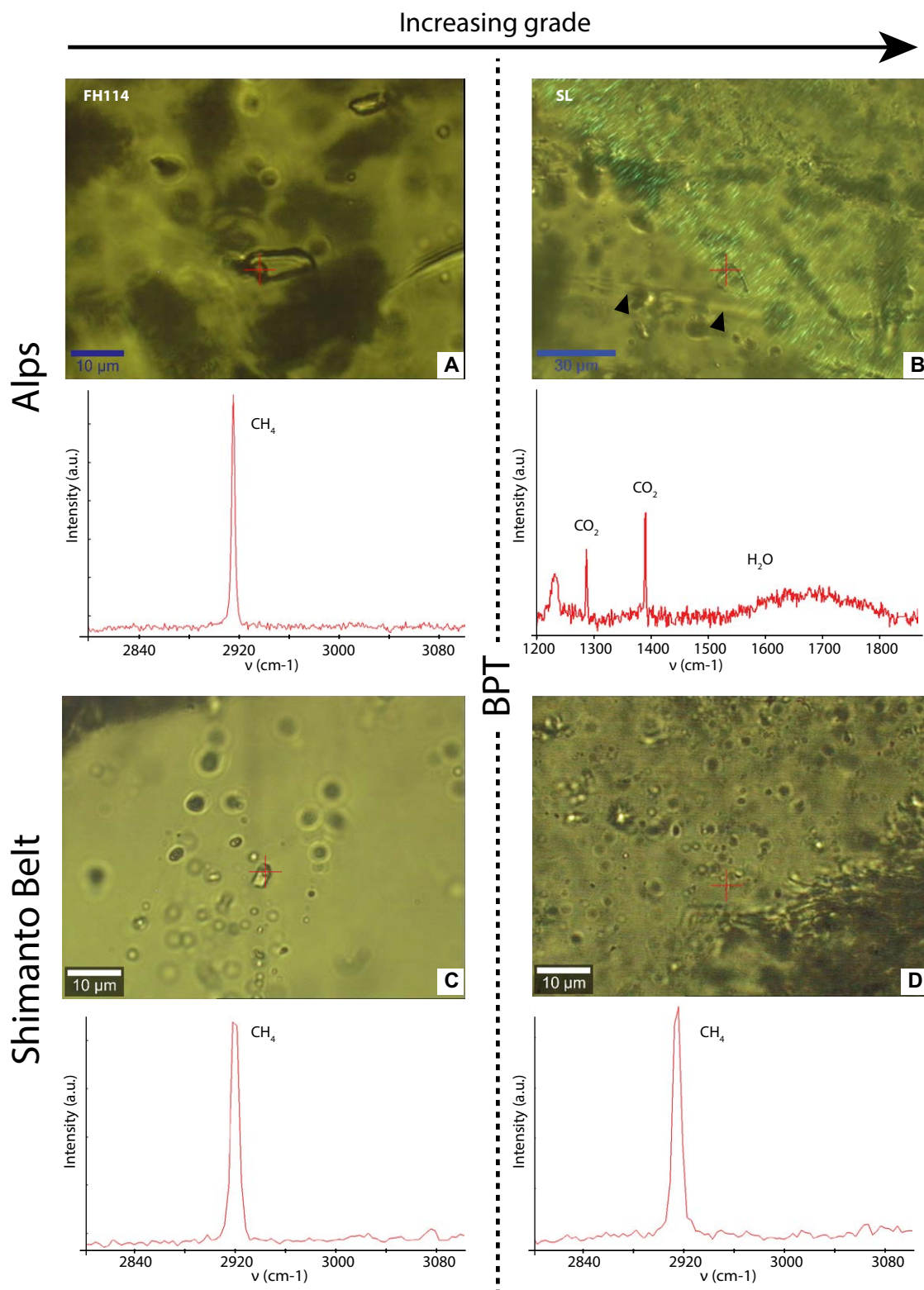


Figure 6. A-A'—Hyuga Tectonic Mélange schistosity-parallel quartz vein, composed of fluid-inclusion-rich, CL-brown, elongated grains (black triangle), crosscut by another vein, constituted of CL-blue, fluid-inclusion-poor quartz vein. B-B'—growth zoning in quartz vein from Flysch à Helminthoïdes (FH) (triangles). Note that the CL-blue quartz is crosscut by smaller, CL-brown cracks (e.g., black triangles), getting locally a ragged or patchy aspect. C-C'—Macro vein in FH, composed of patchy CL-brown and CL-blue quartz. A later-stage and larger set of CL-brown micro-veins cut across the macro-vein. The white line in C stands for the orientation of the vein wall. D-D'—Schistes Lustrés quartz sample with carpholite needle (triangle). E-E'—Folded quartz vein from Foliated Morotsuka. In summary, in high-grade units (D-E), quartz CL color is homogeneously brown, while it alternates CL-blue and CL-brown colors in lower-grade units (A-B-C). Cathodoluminescence (CL) (A-B-C-D-E) and optical microphotographs without crossed nicols (A'-B'-C'-D'-E'). Samples: HN299 (A-A'), FH22 (B-B'), FH13 (C-C'), 10B (D-D'), and HN285 (E-E'). The scale bar at bottom right applies to all images. BPT—brittle-plastic transition.



**Figure 7.** Raman spectra of the gaseous phase in fluid inclusions from the Alps (A: FH; B: SL) and the Shimanto Belt (C: HTM; D: FM). It is composed of methane in all units but the SL, where the bubble is filled with CO<sub>2</sub>. Samples: FH114 (A), 10B (B), HN51 (C), HN145 (D). Abbreviations: BPT—brittle-plastic transition; FH—Flysch à Helminthoïdes; FM—Foliated Morotsuka; HTM—Hyuga Tectonic Mélange; SL—Schistes Lustrés; a.u.—arbitrary units.

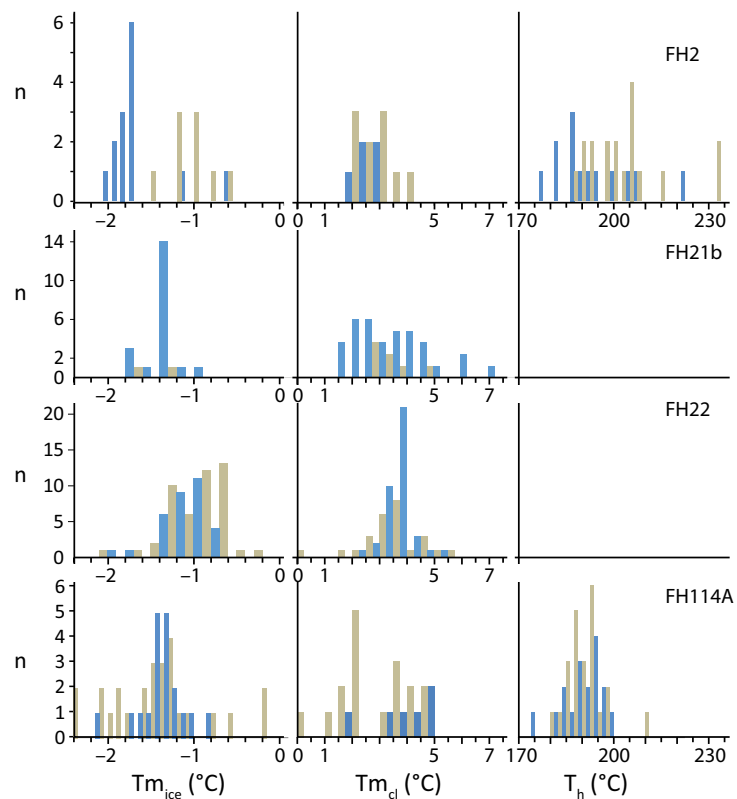


Figure 8. Ice (left), clathrate (middle) melting temperatures, and homogenization temperature (right) for the fluid inclusions in four samples from the Complexe de Base in the Flysch à Helminthoïdes (FH). The two colors blue and brown refer to the cathodoluminescence (CL) color of host quartz. There is no significant difference in any of the microthermometric properties between the CL-blue and CL-brown quartz, except for sample FH2, where  $T_{mi}$  is lower in the CL-blue quartz; hence salinity is higher. Samples: FH2, FH21B, FH22, and FH114A.

Another constraint is provided by the microthermometric record of the fluid inclusions themselves. In FH, homogenization temperatures are concentrated  $\sim 200$  °C, which is slightly lower than the host rock peak temperature of  $270 \pm 30$  °C given by RSCM. In HTM, homogenization temperatures range from 170 to 280 °C, which is also slightly lower or of the order of the host-rock peak temperature of  $245 \pm 30$  °C given by RSCM (Palazzin et al., 2016). In both cases, homogenization temperatures are slightly lower or overlap peak rock temperatures. Trapping temperatures of the fluid are equal to or higher than homogenization temperatures, which even reduces the difference between fluid trapping temperature conditions and rock peak temperature.

TABLE 2. SUMMARY OF MICROTHERMOMETRY MEASUREMENTS FLYSCH À HELMINTHOÏDES

Sample	$T_{mi}$ (°C)		$T_{mcl}$ (°C)		$T_h$ (°C)	
	From	To	From	To	From	To
FH114	-1.5	-1.2	2.6	3.8	180	200
FH2	-2	-0.9	2.2	3.6	175	210
FH21b	-1.2		1.5	5		
FH22	-1.6	-0.6	2.5	4.5		

From structural and microthermometric results, we consider therefore that fluid inclusions in quartz veins from both FH and HTM units formed during the latest stages of burial or even at peak burial and not after. Their record, in terms of fluid P-T conditions, corresponds therefore to the deepest stage of the rock evolution, provided that inclusions were not affected by reequilibration processes during exhumation (see next section).

### Fluid Pressure along the Plate Interface—The Record of Fluid Inclusions

The geological record of near-lithostatic fluid pressure is potentially preserved in fluid inclusions trapped at depth and exhumed along with rocks belonging to paleoplate interfaces. Such a record relies on the assumption that inclusions follow an isochoric path since trapping at high pressure, hence do not reequilibrate. Driving forces for reequilibration (meant as a change in fluid density in the inclusion) are the difference in (1) pressure and (2) water chemical potential between the inclusion and the surrounding crystal (Bakker and Hansen, 1994; Sterner et al., 1995; Bodnar, 2003).

### Reequilibration of Deep Fluid Inclusions

Experimental studies have shown that the assumption of isochoric path is in many cases not valid and that fluid inclusions reequilibrate under both conditions of internal over- and under-pressure (Sterner and Bodnar, 1989; Hall and Sterner, 1993; Vityk and Bodnar, 1995a, 1995b). Several processes account for reequilibration, such as plastic deformation of the inclusion wall (Vityk et al., 2000), leakage through dislocations (Bakker and Hansen, 1994), or fracturing (= decrepitation) of surrounding crystal (Vityk and Bodnar, 1995b).

Indeed, in high-pressure rocks, reequilibration of fluid inclusions during uplift accounts well for the large discrepancy between rock peak P-T conditions in blueschist- or eclogite-facies and the much lower pressure in fluid inclusions trapped concomitantly (Küster and Stöckert, 1997; Agard et al., 2000). The primary reason for such reequilibration can be illustrated in the P-T diagram showing the evolution of fluid-inclusion pressure and rock pressure (Fig. 10), for primary fluid inclusions from the SL trapped concomitantly with high-pressure carpholite (Agard et al., 2000; this study).

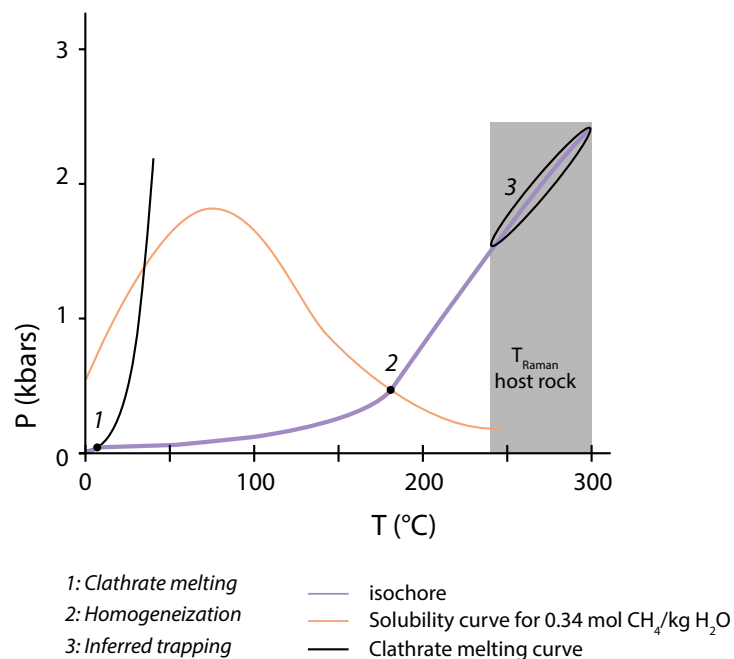


Figure 9. Representative isochore for the fluid inclusions from the Flysch à Helminthoides unit (FH), using values in Table 2 as to get an upper bound on trapping pressure. Trapping conditions are inferred at the intersection between the isochore and the temperature of host rock estimated with Raman (Table 1).

Fluid-inclusion P-T evolution is given by the isochores, which we calculated using equation of state of pure water (Wagner and Pruss, 2002). The actual fluid in the inclusion contains not only water but also a small proportion of gas (CO<sub>2</sub>; see Fig. 7), which should be accounted for in calculating the isochores. Nevertheless, this gaseous phase is much more compressible than water (Duan et al., 1992), which decreases the fluid P-T slope in Figure 10, so that pure-water isochore is an upper bound on actual fluid isochore.

Considering a fluid trapped at peak P-T conditions of the SL (Agard et al., 2000), its isochoric evolution during exhumation follows a slope of  $\sim 3 \times 10^{-2}$  kbar/°C (or equivalently  $\sim 12$  °C/km; red line in Fig. 10). This contrasts with typical upward-concave rock exhumation P-T path, whose first stage follows a much larger P-T slope (blue line in Fig. 10). As a result, during exhumation, there is a divergence between rock and fluid pressure, and internal overpressure develops in the inclusion. The amplitude of overpressure is of a few kbars, that is of the order or larger than what was necessary to trigger reequilibration, in high P and T experiments on Brazilian quartz containing synthetic fluid inclusions (Hall and Sterner, 1993; Vityk and Bodnar, 1995b). In general, it is therefore unlikely that fluid conditions at high-P are preserved.

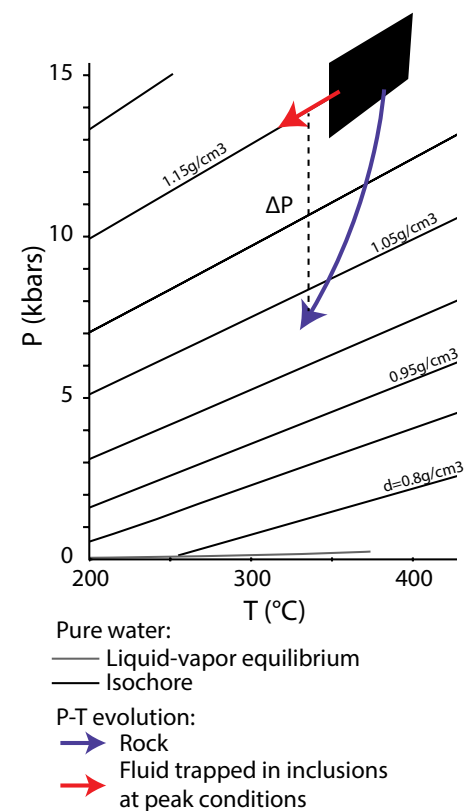


Figure 10. Concomitant evolution of rock (blue) and fluid inclusion (red) pressure-temperature (P-T) conditions during exhumation. The steeper slope of rock P-T path results in large overpressure  $\Delta P$  between the trapped fluid and the surrounding medium, eventually leading in the general case to reequilibrating the fluid. Rock peak conditions (black domain) and exhumation path from the Schistes Lustrés (SL) (Agard et al., 2000), fluid isochores calculated from Wagner and Pruss (2002) for pure water, with associated density. The isochore line passing through the peak P-T conditions corresponds to a T gradient of  $\sim 12$  °C/km.

### Reequilibration of Shallow Fluid Inclusions

The difference in pressure between the fluid inclusions and the surrounding solid medium is the main parameter controlling fluid-inclusion reequilibration. Following this idea, the best preservation of fluid inclusions (hence of the record of their entrapment conditions) is to be expected for units buried to shallower depth (i.e., of the order of seismogenic depths), because the possible divergence between rock and fluid P-T path is then reduced. Furthermore, the T gradient of isochoric lines of pure water ( $\sim 10$ – $15$  °C/km; see Fig. 10) is compatible with the T gradient along some subduction interface (Agard et al., 2009). In some cases, fluid trapped at peak conditions could in principle follow the same P-T exhumation path as rocks without being affected by reequilibration.

The P-T conditions recorded in the fluid inclusions from the present work, as well as a compilation of similar examples from various worldwide accretionary prisms, show nevertheless a discrepancy with respect to the thermal regime in modern subduction zones (Fig. 11). Fluid inclusions record a



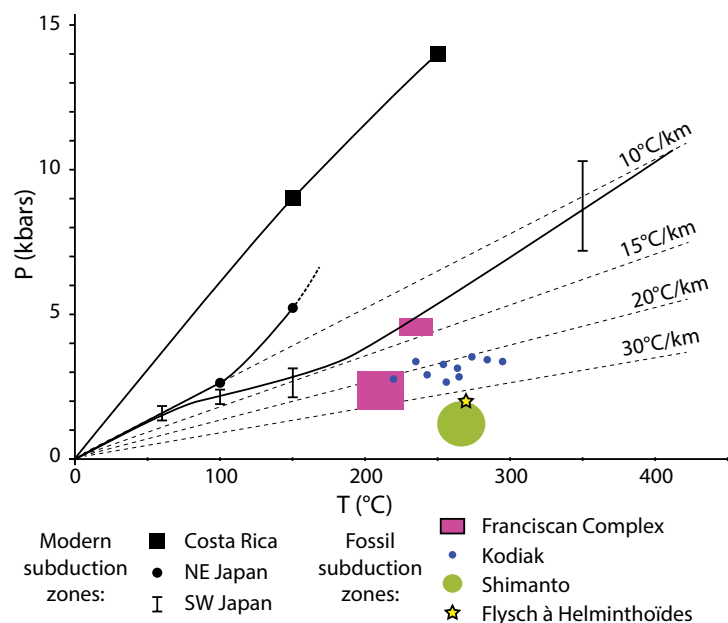


**Figure 11.** Comparison of the pressure-temperature (P-T) record of fluid inclusions in samples corresponding to the seismogenic zone with thermal regimes from modern subduction zones. Fluid inclusions record systematically a lower pressure than along the subduction interface. Reference P-T gradients (dashed lines) were calculated assuming a volumetric mass of 2.65 g/cm<sup>3</sup> for metasediments (Tsuji et al., 2006). References for modern subduction zones: Costa Rica—thermal model from Harris et al. (2010) and plate interface depths from Hayes et al. (2012); NE Japan—Kimura et al. (2012); SW Japan—Marcaillou et al. (2012). References for fossil subduction zones: Franciscan Complex—Dalla Torre et al. (1996); Kodiak—Vrolijk et al. (1988); Shimanto—Raimbourg et al. (2014b); Flysch à Helminthoïdes—this study. Fluid types: Franciscan Complex and Kodiak—methane rich; Shimanto and Flysch à Helminthoïdes—water rich.

lower pressure than all modern zones, including the “hot” subduction zone of SW Japan where the young crust of the Philippines Sea Plate is subducting (Chamot-Rooke et al., 1987; Marcaillou et al., 2012).

Taken at face value, the fluid-inclusion record implies that the fluid pressure is in general significantly lower than the lithostatic pressure near or along the subduction plate interface at depths corresponding to ~200–300 °C, i.e., near the base of the seismogenic zone (Fig. 11). This is possible but would be at variance with geophysical measurements showing large Vp/Vs ratio in this depth domain (Audet et al., 2009; Kato et al., 2010; Audet and Schwartz, 2013; Moreno et al., 2014).

A way out of this discrepancy is to use the fault-valve model (Sibson et al., 1988; Sibson, 1994), where large variations in the fluid pressure occur in relation with the seismic cycle. In such a model, fluid reservoirs, pressurized during the interseismic period, connect in the coseismic stage to shallower aquifers due to earthquake-related damaging. The resulting large-scale fluid

flow leads to transient fluid pressure decrease, before fractures seal, permeability decreases, and fluid pressure increases back to lithostatic values. In this framework, it would be possible that fluid inclusions record principally the low pressure stage of the fluid pressure cycle, i.e., lower values than coeval lithostatic pressure. Experimental studies indicate a significant decrease in quartz solubility when pressure decreases (Anderson and Burnham, 1965), in agreement with the idea of closing cracks and trapping fluid inclusions after pressure drop (Fisher and Brantley, 1992). In addition, in Kodiak accretionary prism (Vrolijk, 1987a, 1987b) and in the Shimanto Belt (Raimbourg et al., 2017), fluid inclusions actually recorded variations in fluid pressure, supporting the model above. Nevertheless, the range of variations is of the order of 1–1.5 kbars, too small to account for the difference between the fluid pressure in the inclusions and the lithostatic pressure along the subduction plane (Fig. 11).

Alternatively, fluid inclusions from the shallower domains of subduction zones could be modified by post entrapment processes, similarly to the deeper domains (4.2.1). This hypothesis is somehow substantiated by the observation that the water-rich fluid inclusions, which are the most common type of fluid inclusions, record the lowest pressure, when compared to coexisting methane-rich fluid inclusions (Sakaguchi, 1999a; Raimbourg et al., 2014b). Because water dissolves the host mineral whereas methane does not, water-rich fluid inclusions are indeed more likely reequilibrated than methane-rich inclusions, which potentially record an internal pressure closer to the pressure of entrapment. One can also note that taking into account the small fraction of methane in the water-rich fluid inclusions (i.e., in the system H<sub>2</sub>O-CH<sub>4</sub>-NaCl), instead of neglecting it as is often done, offsets the isochore toward higher pressure, but to a very limited extent. In the FH (this study) or the Shimanto Belt (Raimbourg et al., 2014b), methane is always present with a low concentration (<1–1.5 mol/L H<sub>2</sub>O), so that this effect becomes negligible, and isochores are similar to pure-water ones and run at very low pressure.

In summary, in the deep domains of subduction zones (blueschists and eclogite facies), the record by fluid inclusions of the fluid pressure is dubious, as postentrapment processes are likely to modify the P-p-T properties of the inclusions in the general case. At shallower depths, corresponding to the seismogenic zone, the record of fluid inclusions is ambiguous. The very low fluid pressure at the time of trapping, with respect to corresponding rock pressure, may reflect the action of reequilibration processes, similarly to the deeper domains. Alternately, fluid inclusions may be systematically trapped after a fluid pressure drop that would be the consequence of the large earthquakes that rupture episodically the plate interface.

### Compositions of the Fluid across the BPT

The low salinity observed in fluid inclusions from the Shimanto Belt or the western Alps is in agreement with other examples of low-grade terranes (Fig. 12), such as the Franciscan Complex (Sadofsky and Bebout, 2001) or the external domain in the Central Alps (Mullis et al., 1994). In Kodiak and nearby Afognak islands, the salinity spans a larger range, which encompasses sea-

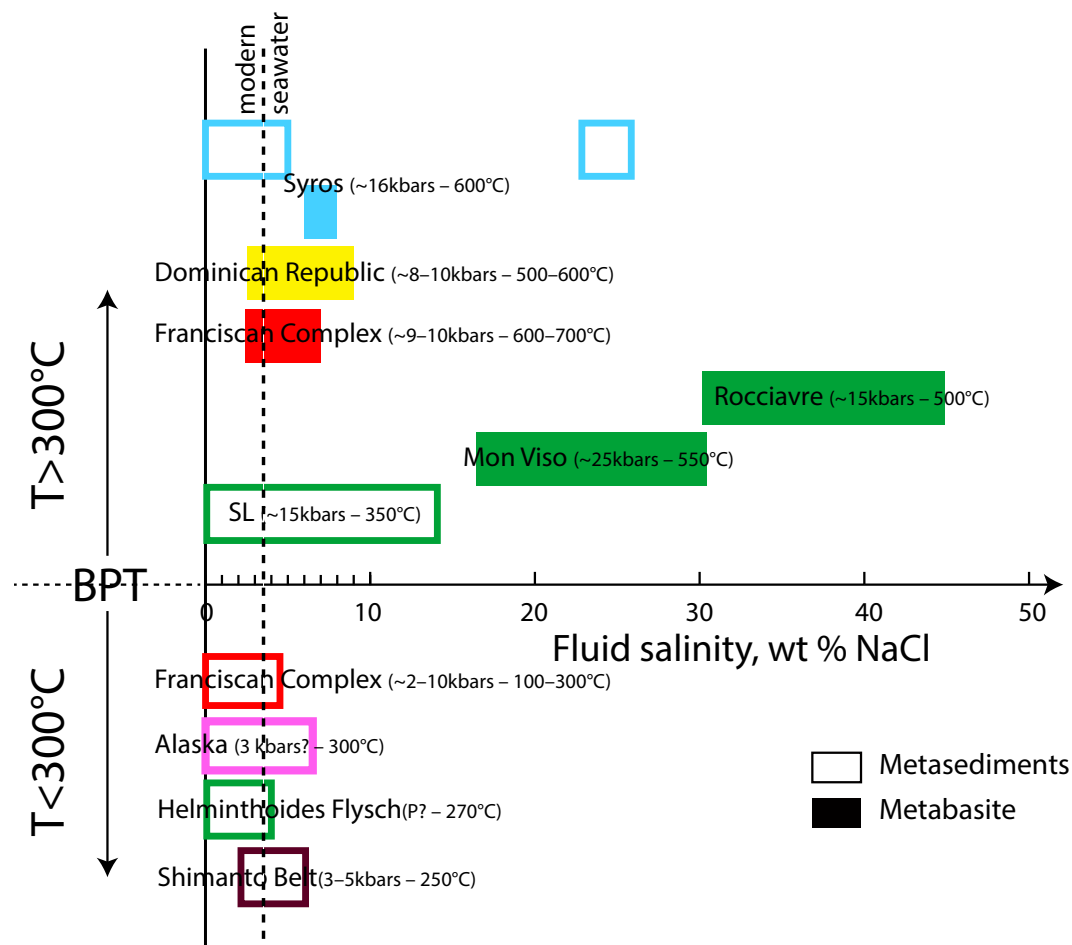


Figure 12. Compilation of salinity in fluid inclusions from metasediments and metabasites in subduction zones. The pressure-temperature (P-T) conditions within brackets correspond to host rock. References: Syros—Barr, 1990; Dominican Republic and Franciscan Complex (deeper than brittle-plastic transition [BPT])—Giaramita and Sorensen, 1994; Mon Viso and Rocciavre—Philippot et al., 1998; Pognante, 1989; Angiboust et al., 2012; Schistes Lustrés (SL)—Vrolijk, 1987a, 1987b; Alaska—Brantley et al., 1998; Agard et al., 2000; Franciscan Complex (shallower than BPT)—Toriumi and Teruya, 1988; Sadofsky and Bebout, 2004; Shimanto Belt—Raimbourg et al., 2014b; this study.

water salinity (Brantley et al., 1998), while the fluid is made of  $H_2O \pm CO_2$ . The transect in the Central Alps by Mullis et al. (1994) shows an increase in salinity from the lower-grade  $CH_4$ - $H_2O$  domain to the higher-grade  $CO_2$ - $H_2O$  domain, with a salinity respectively lower and higher than seawater.

At the much higher conditions of the eclogite facies, the salinity is much more variable, between highly saline brines in serpentine (Scambelluri et al., 1997) and metagabbros (Philippot and Selverstone, 1991) from the Alps and fluid with seawater-like salinity in eclogite blocks from the Franciscan Complex and the Dominican Republic (Giaramita and Sorensen, 1994). This salinity contrast between HP inclusions was interpreted as reflecting initial (= pre-subduction) salinity contrasts by Philippot et al. (1998), but this hypothesis is at

variance with the correlation between salinity and metamorphic grade shown by Mullis et al. (1994) and the relatively homogeneous salinity observed in metasediments shallower than the BPT. The extremely large variability in salinity reported in blueschist-facies metasediments on the island of Syros in the Cyclades (Barr, 1990) is therefore more likely to be connected with local-scale mineral-fluid interactions than with salinity contrasts inherited from the pre-subduction stage.

The nature of the gas dissolved in water shows also a contrasting behavior across the BPT. Shallower than the BPT, the gas phase is predominantly methane, as for example in the Alps (this study), the Shimanto Belt (Sakaguchi, 1999a; this study), or the Franciscan Complex (Sadofsky and Bebout, 2004).

The nature of the dissolved gas phase becomes more variable with increasing depth. In the Alps, where buried sediments are rich in carbonates, the gas phase changes from CH<sub>4</sub> to CO<sub>2</sub> in the T range from 250 to 350 °C (Fig. 7). In contrast, in the Shimanto Belt metasediments, poor in carbonates, the gas phase is still methane at ~350 °C (Fig. 7), except for CO<sub>2</sub>-bearing fluid inclusions in the Muroto Peninsula, associated with Miocene near-trench magmatism (Okamoto et al., 2014). Higher-grade metamorphic rocks are absent from the Shimanto Belt, but in the Jurassic subduction belt of Sambagawa (Japan), also poor in carbonates, all fluid inclusions down to eclogite-facies conditions contain a mixture of water, N<sub>2</sub>, and CH<sub>4</sub>, without any CO<sub>2</sub> (Yoshida et al., 2015). The comparison of the HP domains in the Alps and in the Japanese subduction belts shows how the nature of the host-rock sediment, in particular its concentration in carbonates, controls the nature of the gas dissolved in the water, even if it is unclear which reactions precisely control the release of CO<sub>2</sub> from carbonates (Kerrick and Connolly, 2001; Frezzotti et al., 2011; Cook-Kollars et al., 2014).

In summary, both in terms of salinity and composition of dissolved gas, there is a contrast across the BPT between a relatively homogeneous shallow domain and a much more heterogeneous deep domain. This implies that these two domains are, in terms of fluid, disconnected. It also reflects a relatively open-system behavior of the subducting material shallower than the BPT, contrasting with a closed-system behavior deeper. Such a contrast, in subduction context, is similar to what was observed in context of postorogenic collapse, during the exhumation of terranes along a detachment in the Cycladic islands of Greece (Famin et al., 2004; Famin et al., 2005).

### Model of Fluid Flow along the Plate Interface

In agreement with the geochemical signatures described above, the cathodoluminescence study of quartz veins from the Alps and the Shimanto Belt described here (Fig. 6) reveals a major difference between low- and high-grade domains. While high-grade quartz veins are constituted of a homogeneous, CL-brown material, low-grade veins incorporate, in addition to the CL-brown quartz, a second type of quartz with a bright-blue luminescence. The respective occurrences of CL-blue and CL-brown quartz provide insight into the conditions for their formation. Because CL-blue and CL-brown quartz precipitate in “macro” and “micro” veins (e.g., Figs. 6A and 6B), we interpreted in Raimbourg et al. (2015) the CL-blue and CL-brown quartz as reflecting equilibrium with an external and local fluid, respectively. This interpretation was further supported by the CL-brown color of recrystallized domains in low-grade units, reflecting equilibration with the local fluid wetting the rock (Raimbourg et al., 2015). At high grade, quartz is pervasively recrystallized and homogenized with the local fluid, resulting in a homogeneous CL-brown color.

There is therefore a strong contrast between low-grade units, where episodic influx of external fluid is recorded in fracturing and precipitation of CL-blue quartz, and high-grade units, where the rock evolves as a closed sys-

tem. In terms of mechanical behavior, the transition corresponds to the onset of plastic deformation of quartz (Fig. 4) or, at larger scale, to the seismic-aseismic transition of the plate interface behavior (Byrne et al., 1988; Hyndman et al., 1997; Oleskevich et al., 1999), for temperatures in the range 250–350 °C (Fig. 5 and Table 1).

Similarly to our observations of CL textures in low-grade material, in other examples of subduction thrusts (Vannucchi et al., 2010; Fagereng et al., 2011; Fisher and Brantley, 2014), crack-seal textures have been reported as evidences of repeated events of fracturing, fluid infiltration, and mineral precipitation (Ramsay, 1980). In the mélange zone of the Chrystalls Beach Complex, shear veins with crack-seal textures indicative of displacements of ~10–100 μm were interpreted as the result of repeated micro-earthquakes occurring at ~300 °C, i.e., near the down-dip limit of the subduction thrust (Fagereng et al., 2011). In the Kodiak accretionary complex, in Alaska, veins concentrated near the paleo-décollement record hydraulic events with two distinct timescales: thin veins record repeated crack-seal events (with typical thickness of precipitated quartz of ~8 μm), while a set of thicker veins record less frequent events of fracture porosity collapse (Fisher and Byrne, 1990; Fisher and Brantley, 1992, 2014).

This set of observations leads to a model of circulations with two compartments, limited by the BPT (Fig. 13). Deeper than the BPT, fluid circulation is only local, and the fluid composition (salinity and dissolved gas) is controlled by chemical exchanges with surrounding host rock. Shallower than the BPT, i.e., along the seismogenic zone, stages of closed-system evolution alternate with events of system opening and infiltration of external fluid. The associated fluid has seawater-like or lower salinity and contains dissolved CH<sub>4</sub> with a low concentration.

The connection between these hydrological cycles and the earthquake cycle is unclear, as discussed in Fisher and Brantley (2014). Crack-seal textures may as well result from cyclic variations in pore-fluid pressure, without direct correlation with the seismic slip. The information provided by isotopic studies is also ambiguous. In veins from the Shimanto Belt, Yamaguchi et al. (2011) show a diminution in the fluid redox state during faulting and associated vein precipitation, but their observations cannot distinguish between a transient influx of exotic, deep fluid or the in situ production of hydrogen during seismic faulting. Therefore, further work is necessary to provide clear geological observations connecting the fluid flow to the seismic cycle.

## CONCLUSIONS

Our comparative study of the Alps and the Shimanto Belt, which spans the lower portion of the seismogenic zone and the aseismic, plastic domain at larger depths, shows a relatively contrasted pattern, in terms of fluid circulation, between these two domains. Deeper than the BPT, the system is hydrologically closed, and the quartz, pervasively recrystallized, has a homogeneous, CL-brown color. The fluid salinity is variable and often larger than seawater, and the dissolved gas depends on the host rock. In contrast, shallower than the BPT,

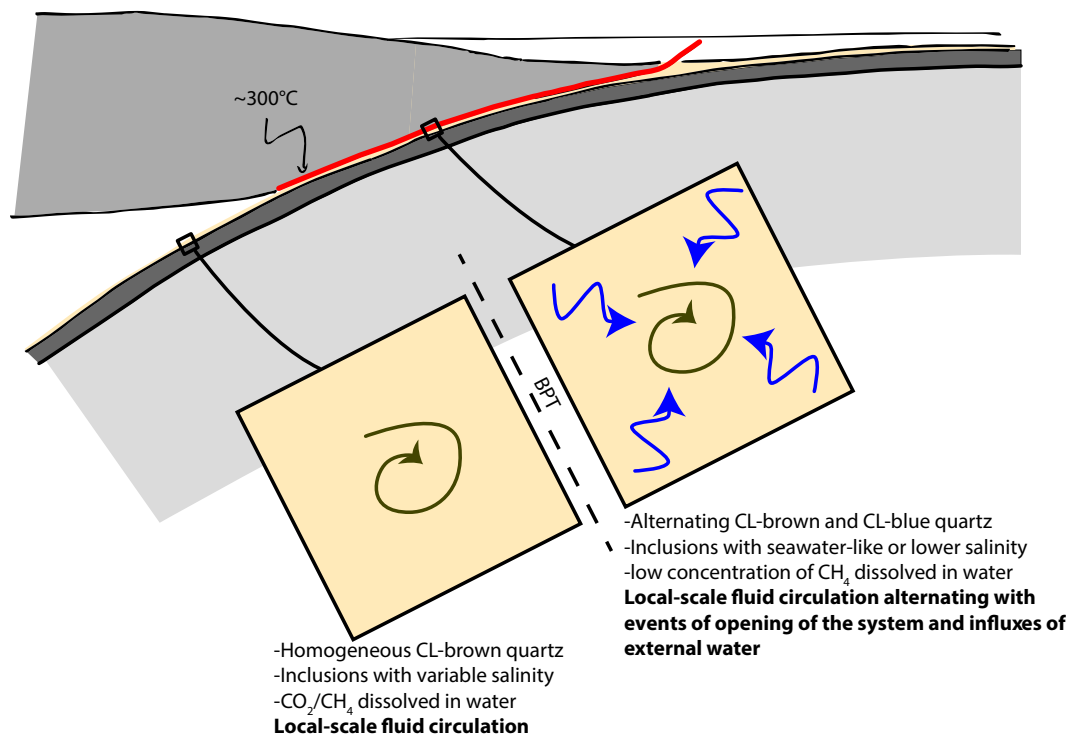


Figure 13. Model of the evolution of the fluid properties and circulation across the brittle-plastic transition (BPT) in sediments along the plate interface. CL – cathodoluminescence.

CL colors reveal the presence of two types of quartz, which we interpret as reflecting hydrological cycles of transient opening and closure of the system. The salinity of the fluid is of the order or lower than seawater, and the dissolved gas is consistently composed of methane, with a low concentration. The seismic cycle constitutes a good candidate for the transient hydrological opening of the system, but further work is required to establish such a connection. In addition, the fluid pressure recorded in fluid inclusions is much lower than lithostatic pressure along the subduction plane, which may reflect either (1) postentrapment, reequilibration processes or (2) trapping of fluid inclusions after a fluid pressure drop that would follow earthquake occurrence.

#### ACKNOWLEDGMENTS

We thank Frédéric Foucher at Centre de Biophysique Moléculaire (CBM), University of Orléans, for Raman analyses and J.G. Badin and S. Janiec for the preparation of thin sections. We also thank Donald Fisher and Åke Fagereng (reviewers) and Philippe Agard (guest associate editor) for their constructive comments, which helped to improve the manuscript. This work has received funding from (1) the European Research Council (ERC) under the seventh Framework Programme of the European Union (ERC Advanced Grant, grant agreement no. 290864, RHEOLITH), (2) the Labex VOLTAIRE (ANR-10-LABX-100-01), and (3) the program “Sakura” by the French Ministry of Foreign Affairs.

#### REFERENCES CITED

- Agard, P., and Lemoine, M., 2003, *Visages des Alpes: Structure et évolution géodynamique*. Paris, Commission de la Carte Géologique du Monde, p. 48.
- Agard, P., Goffé, B., Touret, J.L.R., and Vidal, O., 2000, Retrograde mineral and fluid evolution in high-pressure metapelites (Schistes Lustrés unit, Western Alps): *Contributions to Mineralogy and Petrology*, v. 140, p. 296–315, <https://doi.org/10.1007/s004100000190>.
- Agard, P., Jolivet, L., and Goffé, B., 2001, Tectonometamorphic evolution of the Schistes Lustrés Complex: Implications for the exhumation of HP and UHP rocks in the Western Alps: *Bulletin de la Société Géologique de France*, v. 172, p. 617–636, <https://doi.org/10.2113/172.5.617>.
- Agard, P., Yamato, P., Jolivet, L., and Burov, E., 2009, Exhumation of oceanic blueschists and eclogites in subduction zones: Timing and mechanisms: *Earth-Science Reviews*, v. 92, p. 53–79, <https://doi.org/10.1016/j.earscirev.2008.11.002>.
- Anderson, G.M., and Burnham, C.W., 1965, The solubility of quartz in supercritical water: *American Journal of Science*, v. 263, p. 494–511, <https://doi.org/10.2475/ajs.263.6.494>.
- Angiboust, S., Langdon, R., Agard, P., Waters, D., and Chopin, C., 2012, Eclogitization of the Monviso ophiolite (W. Alps) and implications on subduction dynamics: *Journal of Metamorphic Geology*, v. 30, p. 37–61, <https://doi.org/10.1111/j.1525-1314.2011.00951.x>.
- Audet, P., and Schwartz, S.Y., 2013, Hydrologic control of forearc strength and seismicity in the Costa Rican subduction zone: *Nature Geoscience*, v. 6, p. 852–855, <https://doi.org/10.1038/ngeo1927>.
- Audet, P., Bostock, M.G., Christensen, N.I., and Peacock, S.M., 2009, Seismic evidence for over-pressured subducted oceanic crust and megathrust fault sealing: *Nature*, v. 457, p. 76–78, <https://doi.org/10.1038/nature07650>.

- Bakker, R.J., and Hansen, J.B.H., 1994, A mechanism for preferential H<sub>2</sub>O leakage from fluid inclusions in quartz, based on TEM observations: *Contributions to Mineralogy and Petrology*, v. 116, p. 7–20, <https://doi.org/10.1007/BF00310686>.
- Barr, H., 1990, Preliminary fluid inclusion studies in a high-grade blueschist terrain, Syros, Greece: *Mineralogical Magazine*, v. 54, p. 159–168, <https://doi.org/10.1180/minmag.1990.054.375.03>.
- Bebout, G.E., 1995, The impact of subduction-zone metamorphism on mantle-ocean chemical cycling: *Chemical Geology*, v. 126, p. 191–218, [https://doi.org/10.1016/0009-2541\(95\)00118-5](https://doi.org/10.1016/0009-2541(95)00118-5).
- Bebout, G.E., 2007, Trace element and isotopic fluxes/Subducted slab, 3.20, in Rudnick, R., ed., *The Crust, Treatise on Geochemistry*: Oxford, Elsevier-Perгамon, p. 1–50.
- Bebout, G.E., Agard, P., Kobayashi, K., Moriguti, T., and Nakamura, E., 2013, Devolatilization history and trace element mobility in deeply subducted sedimentary rocks: Evidence from Western Alps HP/UHP suites: *Chemical Geology*, v. 342, p. 1–20, <https://doi.org/10.1016/j.chemgeo.2013.01.009>.
- Bekins, B.A., and Dreiss, S.J., 1992, A simplified analysis of parameters controlling dewatering in accretionary prisms: *Earth and Planetary Science Letters*, v. 109, p. 275–287, [https://doi.org/10.1016/0012-821X\(92\)90092-A](https://doi.org/10.1016/0012-821X(92)90092-A).
- Beyssac, O., Goffé, B., Chopin, C., and Rouzaud, J.N., 2002, Raman spectra of carbonaceous material in metasediments: A new geothermometer: *Journal of Metamorphic Geology*, v. 20, p. 859–871, <https://doi.org/10.1046/j.1525-1314.2002.00408.x>.
- Bodnar, R.J., 2003, Reequilibration of fluid inclusions, in Anderson, A., and Marshall, D., eds., *Fluid Inclusions: Analysis and Interpretation*: Mineralogical Association of Canada, Short Course 32, p. 213–230.
- Bousquet, R.R.O., Goffé, B., Schmid, S.M., and Wiederkehr, M., 2012, *Metamorphic framework of the Alps (1/1,000,000) (second edition)*: Paris, Commission for the Geological Map of the World.
- Brantley, S.L., Fisher, D.M., Deines, P., Clark, M.B., and Myers, G., 1998, Segregation veins: Evidence for the deformation and dewatering of a low-grade metapelite, in Holness, M.B., ed., *Deformation-Enhanced Fluid Transport in the Earth's crust and mantle*: London, Chapman and Hall, p. 267–288.
- Breeding, C.M., and Ague, J.J., 2002, Slab-derived fluids and quartz vein formation in an accretionary prism, Otago Schist, New Zealand: *Geology*, v. 30, p. 499–502, [https://doi.org/10.1130/0091-7613\(2002\)030<0499:SDFAQV>2.0.CO;2](https://doi.org/10.1130/0091-7613(2002)030<0499:SDFAQV>2.0.CO;2).
- Busigny, V., Cartigny, P., Philippot, P., Ader, M., and Javoy, M., 2003, Massive recycling of nitrogen and other fluid-mobile elements in a cold slab environment: Evidence from HP to UHP oceanic metasediments of the Schistes Lustrés nappe (Western Alps, Europe): *Earth and Planetary Science Letters*, v. 215, p. 27–42, [https://doi.org/10.1016/S0012-821X\(03\)00453-9](https://doi.org/10.1016/S0012-821X(03)00453-9).
- Byrne, T., and Fisher, D., 1990, Evidence for a weak and overpressured décollement beneath sediment-dominated accretionary prisms: *Journal of Geophysical Research*, v. 95, p. 9081–9097, <https://doi.org/10.1029/JB095iB06p09081>.
- Byrne, D.E., Davis, D.M., and Sykes, L.R., 1988, Loci and maximum size of thrust earthquakes and the mechanics of the shallow region of subduction zones: *Tectonics*, v. 7, p. 833–857, <https://doi.org/10.1029/TC007i004p00833>.
- Caby, R., Kienast, J.R., and Salot, P., 1978, Structure, métamorphisme et modèle d'évolution tectonique des Alpes Occidentales: *Revue de Géographie Physique et de Géologie Dynamique*, v. 20, p. 307–322.
- Caron, C., Hesse, R., Kerckhove, C., Homewood, P., Van Stuijvenberg, J., Tasse, N., and Winkler, W., 1981, Comparaison préliminaire des flyschs à Helminthoïdes sur trois transversales des Alpes: *Eclogae Geologicae Helvetiae*, v. 74, p. 369–378.
- Caron, J.-M., 1977, Evolution paléogéographique et tectonique de la zone piémontaise dans les Alpes cottiennes: *Bulletin de la Société Géologique de France*, v. 19, no. 4, p. 893–899, doi: 10.2113/gssgfbull.S7-XIX.4.893.
- Chamot-Rooke, N., Renard, V., and Pichon, X.L., 1987, Magnetic anomalies in the Shikoku Basin: A new interpretation: *Earth and Planetary Science Letters*, v. 83, p. 214–228, [https://doi.org/10.1016/0012-821X\(87\)90067-7](https://doi.org/10.1016/0012-821X(87)90067-7).
- Chopin, C., and Schreyer, W., 1983, Magnesiochloritoid and magnesiochloritoid: Two index minerals and their preliminary phase relations in the model system MgO-Al<sub>2</sub>O<sub>3</sub>-SiO<sub>2</sub>-H<sub>2</sub>O: *American Journal of Science*, v. 280, p. 72–96.
- Cook-Kollars, J., Bebout, G.E., Collins, N.C., Angiboust, S., and Agard, P., 2014, Subduction zone metamorphic pathway for deep carbon cycling: I. Evidence from HP/UHP metasedimentary rocks, Italian Alps: *Chemical Geology*, v. 386, p. 31–48, <https://doi.org/10.1016/j.chemgeo.2014.07.013>.
- Dalla Torre, M., De Capitani, C., Frey, M., Underwood, M., Mullis, J., and Cox, R., 1996, Very low-temperature metamorphism of shales from the Diablo Range, Franciscan Complex, California: New constraints on the exhumation path: *Geological Society of America Bulletin*, v. 108, p. 578–601, [https://doi.org/10.1130/0016-7606\(1996\)108<0578:VLTMO>2.3.CO;2](https://doi.org/10.1130/0016-7606(1996)108<0578:VLTMO>2.3.CO;2).
- Duan, Z., Moller, N., and Weare, J.H., 1992, An equation of state for the CH<sub>4</sub>-CO<sub>2</sub>-H<sub>2</sub>O system: I. Pure systems from 0 to 1000°C and 0 to 8000 bar: *Geochimica et Cosmochimica Acta*, v. 56, p. 2605–2617, [https://doi.org/10.1016/0016-7037\(92\)90347-L](https://doi.org/10.1016/0016-7037(92)90347-L).
- Duarte, J.C., Schellart, W.P., and Cruden, A.R., 2015, How weak is the subduction zone interface: *Geophysical Research Letters*, v. 42, p. 1–10, <https://doi.org/10.1002/2014GL062876>.
- Eberhart-Phillips, D., Reyners, M., Chadwick, M., and Chiu, J.-M., 2005, Crustal heterogeneity and subduction processes: 3-D Vp, Vp/Vs and Q in the southern North Island, New Zealand: *Geophysical Journal International*, v. 162, p. 270–288, <https://doi.org/10.1111/j.1365-246X.2005.02530.x>.
- El Mekki-Azouzi, M., 2010, *Etude expérimentale de l'eau et des solutions aqueuses métastables—Implications pour le milieu naturel* [Ph.D. thesis]: Orléans, Université d'Orléans, 259 p.
- Erickson, S.N., and Jarrard, R.D., 1998, Velocity-porosity relationships for water-saturated siliclastic sediments: *Journal of Geophysical Research*, v. 103, p. 30,385–30,406.
- Faccenna, C., Becker, T.W., Lallemand, S., and Steinberger, B., 2012, On the role of slab pull in the Cenozoic motion of the Pacific plate: *Geophysical Research Letters*, v. 39, L03305, <https://doi.org/10.1029/2011GL050155>.
- Fagereng, A., and Harris, C., 2014, Interplay between fluid flow and fault-fracture mesh generation within underthrust sediments: Geochemical evidence from the Chrystalls Beach Complex, New Zealand: *Tectonophysics*, v. 612–613, p. 147–157, <https://doi.org/10.1016/j.tecto.2013.12.002>.
- Fagereng, A., Remitti, F., and Sibson, R.H., 2011, Incrementally developed slickenfibers—Geological record of repeating low stress-drop seismic events?: *Tectonophysics*, v. 510, p. 381–386, <https://doi.org/10.1016/j.tecto.2011.08.015>.
- Famin, V., Philippot, P., Jolivet, L., and Agard, P., 2004, Evolution of hydrothermal regime along a crustal shear zone, Tinos Island, Greece: *Tectonics*, v. 23, TC5004, <https://doi.org/10.1029/2003TC001509>.
- Famin, V., Hébert, R., Philippot, P., and Jolivet, L., 2005, Ion probe and fluid inclusion evidence for co-seismic fluid infiltration in a crustal detachment: *Contributions to Mineralogy and Petrology*, v. 150, p. 354–367, <https://doi.org/10.1007/s00410-005-0031-x>.
- Ferry, J.M., and Dipple, G.M., 1991, Fluid flow, mineral reactions, and metasomatism: *Geology*, v. 19, p. 211–214, [https://doi.org/10.1130/0091-7613\(1991\)019<0211:FFMRAM>2.3.CO;2](https://doi.org/10.1130/0091-7613(1991)019<0211:FFMRAM>2.3.CO;2).
- Fisher, D., and Byrne, T., 1987, Structural evolution of underthrust sediments, Kodiak Islands, Alaska: *Tectonics*, v. 6, no. 6, p. 775–793, <https://doi.org/10.1029/TC006i006p00775>.
- Fisher, D., and Byrne, T., 1990, The character and distribution of mineralized fractures in the Kodiak Formation, Alaska: Implications for fluid flow in an underthrust sequence: *Journal of Geophysical Research: Solid Earth*, v. 95, no. B6, p. 9069–9080, <https://doi.org/10.1029/JB095iB06p09069>.
- Fisher, D.M., and Brantley, S.L., 1992, Models of quartz overgrowth and vein formation: Deformation and episodic fluid flow in an ancient subduction zone: *Journal of Geophysical Research*, v. 97, p. 20,043–20,061.
- Fisher, D.M., and Brantley, S.L., 2014, The role of silica redistribution in the evolution of slip instabilities along subduction interfaces: Constraints from the Kodiak accretionary complex, Alaska: *Journal of Structural Geology*, v. 69, p. 395–414, <https://doi.org/10.1016/j.jsg.2014.03.010>.
- Fisher, D.M., Brantley, S.L., Everett, M., and Dzonik, J., 1995, Cyclic fluid flow through a regionally extensive fracture network within the Kodiak accretionary prism: *Journal of Geophysical Research*, v. 100, p. 12,881–812,894.
- Frezzotti, M.L., Selverstone, J., Sharp, Z.D., and Compagnoni, R., 2011, Carbonate dissolution during subduction revealed by diamond-bearing rocks from the Alps: *Nature Geoscience*, v. 4, p. 703–706, <https://doi.org/10.1038/ngeo1246>.
- Fukuchi, R., Fujimoto, K., Kameda, J., Hamahashi, M., Yamaguchi, A., Kimura, G., Hamada, Y., Hashimoto, Y., Kitamura, Y., and Saito, S., 2014, Changes in illite crystallinity within an ancient tectonic boundary thrust caused by thermal, mechanical, and hydrothermal effects: An example from the Nobeoka Thrust, southwest Japan: *Earth, Planets, and Space*, v. 66, no. 116, p. 1–12.
- Giaramita, M.J., and Sorensen, S.S., 1994, Primary fluids in low-temperature eclogites: Evidence from two subduction complexes (Dominican Republic, and California, USA): *Contributions to Mineralogy and Petrology*, v. 117, p. 279–292, <https://doi.org/10.1007/BF00310869>.

- Goffé, B., and Chopin, C., 1986, High-pressure metamorphism in the Western Alps: Zoneography of metapelites, chronology and consequences: *Schweiz, Mineralogische und Petrographische Mitteilungen*, v. 66, p. 41–52.
- Hall, D.L., and Sterner, S.M., 1993, Preferential water loss from synthetic fluid inclusions: Contributions to Mineralogy and Petrology, v. 114, p. 489–500, <https://doi.org/10.1007/BF00321753>.
- Harris, R.N., Spinelli, G., Ranero, C.R., Grevemeyer, I., Villinger, H.W., and Barchhausen, U., 2010, Thermal regime of the Costa Rican convergent margin: 2. Thermal models of the shallow Middle America subduction zone offshore Costa Rica: *Geochemistry Geophysics Geosystems*, v. 11, Q12S29, <https://doi.org/10.1029/2010GC003273>.
- Hasegawa, A., Yoshida, K., Asano, Y., Okada, T., Iinuma, T., and Ito, Y., 2012, Change in stress field after the 2011 great Tohoku-Oki earthquake: *Earth and Planetary Science Letters*, v. 355–356, p. 231–243, <https://doi.org/10.1016/j.epsl.2012.08.042>.
- Hayes, G.P., Wald, D.J., and Johnson, R.L., 2012, Slab 1.0: A three-dimensional model of global subduction zone geometries: *Journal of Geophysical Research*, v. 117, B01302, <https://doi.org/10.1029/2011JB008524>.
- Henry, P., Foucher, J.-P., Le Pichon, X., Sibuet, M., Kobayashi, K., Tarits, P., Chamot-Rooke, N., Furuta, T., and Schultheiss, P., 1992, Interpretation of temperature measurements from the Kaiko-Nankai cruise: Modeling of fluid flow in clam colonies: *Earth and Planetary Science Letters*, v. 109, p. 355–371, [https://doi.org/10.1016/0012-821X\(92\)90098-G](https://doi.org/10.1016/0012-821X(92)90098-G).
- Hyndman, R.D., Yamano, M., and Oleskevich, D.A., 1997, The seismogenic zone of subduction thrust faults: The Island Arc, v. 6, p. 244–260, <https://doi.org/10.1111/j.1440-1738.1997.tb00175.x>.
- Jarrard, R.D., 2003, Subduction fluxes of water, carbon dioxide, chlorine, and potassium: *Geochemistry, Geophysics, Geosystems*, v. 4, no. 5, 8905, <https://doi.org/10.1029/2002GC000392>.
- Kastner, M., Elderfield, H., and Martin, J.B., 1991, Fluids in convergent margins: What do we know about their composition, origin, role in diagenesis and importance for oceanic chemical fluxes?: *Philosophical Transactions of the Royal Society of London. Series B, Biological Sciences*, v. 335, p. 243–259.
- Kato, A., Iidaka, T., Ikuta, R., Yoshida, Y., et al., 2010, Variations of fluid pressure within the subducting oceanic crust and slow earthquakes: *Geophysical Research Letters*, v. 37, L14310, <https://doi.org/10.1029/2010GL043723>.
- Kawabata, K., Tanaka, H., and Kimura, G., 2007, Mass transfer and pressure solution in deformed shale of accretionary complex: Examples from the Shimanto Belt, southwestern Japan: *Journal of Structural Geology*, v. 29, p. 697–711, <https://doi.org/10.1016/j.jsg.2006.11.009>.
- Kerckhove, C., 1963, Schéma structural de la nappe du Flysch à Helminthoïdes dans l'Embrunais-Ubaye: *Grenoble, Travaux du Laboratoire de Géologie de Grenoble*, v. 39, p. 7–24.
- Kerckhove, C., 1969, La "Zone du Flysch" dans les nappes de l'Embrunais-Ubaye (Alpes occidentales): *Géologie Alpine*, v. 45, p. 1–202.
- Kerckhove, C., Barfety, J.-C., Bogdanoff, S., and Lemoine, M., 1980, Carte géologique de la France 1:250,000, Feuille de Gap: Orléans, Bureau de Recherches Géologiques et Minières, Map 35.
- Kerckhove, C., Gidon, M., and Pairis, J.L., 2005, Carte géologique de la France (1/50000) feuille Embrun-Guilleville (2ème édition, coupure spéciale) (871): Orléans, Bureau de Recherches Géologiques et Minières.
- Kerrick, D.M., and Connolly, J.A.D., 2001, Metamorphic devolatilization of subducted marine sediments and the transport of volatiles into the Earth's mantle: *Nature*, v. 411, p. 293–296, <https://doi.org/10.1038/35077056>.
- Kimura, G., Hina, S., Hamada, Y., Kameda, J., Tsuji, T., Kinoshita, M., and Yamaguchi, A., 2012, Runaway slip to the trench due to rupture of highly pressurized megathrust beneath the middle trench slope: The tsunamigenesis of the 2011 Tohoku earthquake off the east coast of northern Japan: *Earth and Planetary Science Letters*, v. 339–340, p. 32–45, <https://doi.org/10.1016/j.epsl.2012.04.002>.
- Kitajima, H., and Saffer, D.M., 2012, Elevated pore pressure and anomalously low stress in regions of low frequency earthquakes along the Nankai Trough subduction megathrust: *Geophysical Research Letters*, v. 39, L23301, <https://doi.org/10.1029/2012GL053793>.
- Kondo, H., Kimura, G., Masago, H., Ohmori-Ikehara, K., Kitamura, Y., Ikesawa, E., Sakaguchi, A., Yamaguchi, A., and Okamoto, S., 2005, Deformation and fluid flow of a major out-of-sequence thrust located at seismogenic depth in an accretionary complex: Nobeoka Thrust in the Shimanto Belt, Kyushu, Japan: *Tectonics*, v. 24, TC6008, <https://doi.org/10.1029/2004TC001655>.
- Küster, M., and Stöckert, B., 1997, Density changes of fluid inclusions in high-pressure low-temperature metamorphic rocks from Crete: A thermobarometric approach based on the creep strength of the host minerals: *Lithos*, v. 41, p. 151–167, [https://doi.org/10.1016/S0024-4937\(97\)82010-5](https://doi.org/10.1016/S0024-4937(97)82010-5).
- Lahfid, A., Beyssac, O., Deville, E., Negro, F., Chopin, C., and Goffé, B., 2010, Evolution of the Raman spectrum of carbonaceous material in low-grade metasediments of the Glarus Alps (Switzerland): *Terra Nova*, v. 22, p. 354–360, <https://doi.org/10.1111/j.1365-3121.2010.00956.x>.
- Lamb, S., 2006, Shear stresses on megathrusts: Implications for mountain building behind subduction zones: *Journal of Geophysical Research*, v. 111, B07401, <https://doi.org/10.1029/2005JB003916>.
- Lemoine, M., Bas, T., Arnaud-Vanneau, A., Arnaud, H., Dumont, T., Gidon, M., Bourbon, M., De Graciansky, P.C., Rudkiewicz, J.L., Megard-Galli, J., and Tricart, P., 1986, The continental margin of the Mesozoic Tethys in the Western Alps: *Marine and Petroleum Geology*, v. 3, p. 179–199, [https://doi.org/10.1016/0264-8172\(86\)90044-9](https://doi.org/10.1016/0264-8172(86)90044-9).
- Le Pichon, X., Henry, P., and Lallemand, S., 1993, Accretion and erosion in subduction zones: The role of fluids: *Annual Review of Earth and Planetary Sciences*, v. 21, p. 307–331, <https://doi.org/10.1146/annurev.ea.21.050193.001515>.
- Lewis, J.C., and Byrne, T.B., 2003, History of metamorphic fluids along outcrop-scale faults in a Paleogene accretionary prism, SW Japan: Implications for prism-scale hydrology: *Geochemistry Geophysics Geosystems*, v. 4, 9007, <https://doi.org/10.1029/2002GC000359>.
- Marcaillou, B., Henry, P., Kinoshita, M., et al., 2012, Seismogenic zone temperatures and heat-flow anomalies in the To-nankai margin segment based on temperature data from IODP expedition 333 and thermal model: *Earth and Planetary Science Letters*, v. 349–350, p. 171–185, <https://doi.org/10.1016/j.epsl.2012.06.048>.
- Matsumura, M., Hashimoto, Y., Kimura, G., Ohmori-Ikehara, K., Enjohji, M., and Ikesawa, E., 2003, Depth of oceanic-crust underplating in a subduction zone: Inferences from fluid-inclusion analyses of crack-seal veins: *Geology*, v. 31, p. 1005–1008, <https://doi.org/10.1130/G19885.1>.
- Meneghini, F., and Moore, J.C., 2007, Deformation and hydrofracture in a subduction thrust at seismogenic depths: The Rodeo Cove thrust zone, Marin Headlands, California: *Geological Society of America Bulletin*, v. 119, p. 174–183, <https://doi.org/10.1130/B25807.1>.
- Meneghini, F., Marroni, M., and Pandolfi, L., 2007, Fluid flow during accretion in sediment-dominated margins: Evidence of a high-permeability fossil fault zone from the Internal Ligurian accretionary units of the Northern Apennines, Italy: *Journal of Structural Geology*, v. 29, p. 515–529, <https://doi.org/10.1016/j.jsg.2006.10.003>.
- Merle, O., 1982, Mise en place séquentielle de la Nappe du Parpaillon en Embrunais-Ubaye (Flysch à Helminthoïdes, Alpes occidentales): *Paris, Comptes rendus de l'Académie des Sciences, série II*, v. 294, p. 603–606.
- Merle, O., and Brun, J.P., 1981, La déformation polyphasé de la Nappe du Parpaillon (Flysch à Helminthoïdes): Un résultat de la déformation progressive associée à une translation non rectiligne: *Paris, Comptes rendus de l'Académie des Sciences, série II*, v. 292, p. 343–346.
- Michard, A., Goffé, B., Chopin, C., and Henry, C., 1996, Did the Western Alps develop through an Oman-type stage?: The geotectonic setting of high-pressure metamorphism in two contrasting Tethyan transects: *Eclogae Geologicae Helvetiae*, v. 89, p. 43–80.
- Moore, J.C., and Saffer, D., 2001, Updip limit of the seismogenic zone beneath the accretionary prism of southwest Japan: An effect of diagenetic to low-grade metamorphic processes and increasing effective stress: *Geology*, v. 29, p. 183–186, [https://doi.org/10.1130/0091-7613\(2001\)029<0183:ULOTSZ>2.0.CO;2](https://doi.org/10.1130/0091-7613(2001)029<0183:ULOTSZ>2.0.CO;2).
- Moreno, M., Haberland, C., Oncken, O., Rietbrock, A., Angiboust, S., and Heidbach, O., 2014, Locking of the Chile subduction zone controlled by fluid pressure before the 2010 earthquake: *Nature Geoscience*, v. 7, p. 292–296, <https://doi.org/10.1038/ngeo2102>.
- Mullis, J., Dubessy, J., Poty, B., and O'Neil, J., 1994, Fluid regimes during late stages of a continental collision: Physical, chemical, and stable isotope measurements of fluid inclusions in fissure quartz from a geotraverse in the Central Alps, Switzerland: *Geochimica et Cosmochimica Acta*, v. 58, p. 2239–2267, [https://doi.org/10.1016/0016-7037\(94\)90008-6](https://doi.org/10.1016/0016-7037(94)90008-6).
- Murata, A., 1997, Geological map of Miyazaki prefecture, 1:200,000: Miyazaki Prefectural Government.
- Neuzil, C.E., 1994, How permeable are clays and shales?: *Water Resources Research*, v. 30, p. 145–150, <https://doi.org/10.1029/93WR02930>.
- Okamoto, A., Musya, M., Hashimoto, Y., and Tsuchiya, N., 2014, Distribution of CO<sub>2</sub> fluids in the Shimanto belt on Muroto Peninsula, SW Japan: Possible injection of magmatic CO<sub>2</sub> into the accretionary prism: *Earth, Planets, and Space*, v. 66, p. 1–9, <https://doi.org/10.1186/1880-5981-66-33>.

- Oleskevich, D.A., Hyndman, R.D., and Wang, K., 1999, The updip and downdip limits to great subduction earthquakes: Thermal and structural models of Cascadia, south Alaska, SW Japan, and Chile: *Journal of Geophysical Research*, v. 104, p. 14965–14991, <https://doi.org/10.1029/1999JB900060>.
- Palazzin, G., Raimbourg, H., Famin, V., Jolivet, L., Kusaba, Y., and Yamaguchi, A., 2016, Deformation processes at the down-dip limit of the seismogenic zone: The example of Shimanto accretionary complex: *Tectonophysics*, v. 687, p. 28–43, <https://doi.org/10.1016/j.tecto.2016.08.013>.
- Philippot, P., and Selverstone, J., 1991, Trace-element-rich brines in eclogitic veins: Implications for fluid composition and transport during subduction: *Contributions to Mineralogy and Petrology*, v. 106, p. 417–430, <https://doi.org/10.1007/BF00321985>.
- Philippot, P., Agrinier, P., and Scambelluri, M., 1998, Chlorine cycling during subduction of altered oceanic crust: *Earth and Planetary Science Letters*, v. 161, p. 33–44, [https://doi.org/10.1016/S0012-821X\(98\)00134-4](https://doi.org/10.1016/S0012-821X(98)00134-4).
- Plank, T., and Langmuir, C.H., 1998, The chemical composition of subducting sediment and its consequences for the crust and mantle: *Chemical Geology*, v. 145, p. 325–394, [https://doi.org/10.1016/S0009-2541\(97\)00150-2](https://doi.org/10.1016/S0009-2541(97)00150-2).
- Pognante, U., 1989, Early Alpine eclogitisation in talc/chloritoid-bearing Mg-metagabbros and in jadeite-Fe-omphacite-bearing metatrandhjemites from the ophiolites of the Western Alps: *Rendiconti della Società Italiana di Mineralogia e Petrologia*, v. 43, p. 687–704.
- Raimbourg, H., Shibata, T., Yamaguchi, A., Yamaguchi, H., and Kimura, G., 2009, Horizontal shortening versus vertical loading in accretionary prisms: *Geochemistry Geophysics Geosystems*, v. 10, Q04007, <https://doi.org/10.1029/2008GC002279>.
- Raimbourg, H., Hamano, Y., Saito, S., Kinoshita, M., and Kopf, A., 2011, Acoustic and mechanical properties of Nankai accretionary prism core samples: *Geochemistry Geophysics Geosystems*, v. 12, Q0AD10, <https://doi.org/10.1029/2010GC003169>.
- Raimbourg, H., Augier, R., Famin, V., Gadenne, L., Palazzin, G., Yamaguchi, A., and Kimura, G., 2014a, Long-term evolution of an accretionary prism: The case study of the Shimanto Belt, Kyushu, Japan: *Tectonics*, v. 33, p. 936–959, <https://doi.org/10.1002/2013TC003412>.
- Raimbourg, H., Thiery, R., Vacelet, M., Ramboz, C., Cluzel, N., Trong, E.L., Yamaguchi, A., and Kimura, G., 2014b, A new method of reconstituting the P-T conditions of fluid circulation in an accretionary prism (Shimanto, Japan) from microthermometry of methane-bearing aqueous inclusions: *Geochimica et Cosmochimica Acta*, v. 125, p. 96–109, <https://doi.org/10.1016/j.gca.2013.09.025>.
- Raimbourg, H., Vacelet, M., Ramboz, C., Famin, V., Augier, R., Palazzin, G., Yamaguchi, A., and Kimura, G., 2015, Fluid circulation in the depths of accretionary prisms: An example of the Shimanto Belt, Kyushu, Japan: *Tectonophysics*, v. 655, p. 161–176, <https://doi.org/10.1016/j.tecto.2015.05.023>.
- Raimbourg, H., Thiéry, R., Vacelet, M., Famin, V., Ramboz, C., Boussafir, M., Disnar, J.-R., and Yamaguchi, A., 2017, Organic matter cracking: A source of fluid overpressure in subducting sediments: *Tectonophysics*, v. 721, p. 254–274, <https://doi.org/10.1016/j.tecto.2017.08.005>.
- Ramsay, J.G., 1980, The crack-seal mechanism of rock deformation: *Nature*, v. 284, p. 135–139, <https://doi.org/10.1038/284135a0>.
- Ranero, C.R., Morgan, J.P., McIntosh, K., and Reichert, C., 2003, Bending-related faulting and mantle serpentinization at the Middle America trench: *Nature*, v. 425, p. 367–373, <https://doi.org/10.1038/nature01961>.
- Sadofsky, S.J., and Bebout, G.E., 2001, Paleohydrology at 5- to 50-kilometer depths of accretionary prisms: The Franciscan Complex, California: *Geophysical Research Letters*, v. 28, p. 2309–2312, <https://doi.org/10.1029/2000GL008533>.
- Sadofsky, S.J., and Bebout, G.E., 2003, Record of forearc devolatilization in low-T, high-P/T metasedimentary suites: Significance for models of convergent margin chemical cycling: *Geochemistry Geophysics Geosystems*, v. 4, p. 29, <https://doi.org/10.1029/2002GC000412>.
- Sadofsky, S.J., and Bebout, G.E., 2004, Field and isotopic evidence for fluid mobility in the Franciscan Complex: Forearc paleohydrogeology to depths of 30 kilometers: *International Geology Review*, v. 46, p. 1053–1088, <https://doi.org/10.2747/0020-6814.46.12.1053>.
- Saffer, D.M. and Bekins, B.A., 1998, Episodic fluid flow in the Nankai accretionary complex: Timescale, geochemistry, flow rates and fluid budget: *Journal of Geophysical Research*, v. 103, no. B12, p. 30,351–30,370.
- Saffer, D.M., and Tobin, H.J., 2011, Hydrogeology and mechanics of subduction zone forearcs: Fluid flow and pore pressure: *Annual Review of Earth and Planetary Sciences*, v. 39, p. 157–186, <https://doi.org/10.1146/annurev-earth-040610-133408>.
- Saito, M., Kimura, K., Naito, K., and Sakai, A., 1996, Geological Map of Japan, 1:50,000: Shiibamura, Geological Survey of Japan.
- Saito, M., Sakaguchi, K., and Komazawa, M., 1997, Geological Map of Japan, 1:200,000: Miyazaki, Geological Survey of Japan.
- Sakaguchi, A., 1996, High paleogeothermal gradient with ridge subduction beneath the Cretaceous Shimanto accretionary prism, southwest Japan: *Geology*, v. 24, p. 795–798, [https://doi.org/10.1130/0091-7613\(1996\)024<0795:HPGWRS>2.3.CO;2](https://doi.org/10.1130/0091-7613(1996)024<0795:HPGWRS>2.3.CO;2).
- Sakaguchi, A., 1999a, Thermal maturity in the Shimanto accretionary prism, southwest Japan, with the thermal change of the subducting slab: Fluid inclusion and vitrinite reflectance study: *Earth and Planetary Science Letters*, v. 173, p. 61–74, [https://doi.org/10.1016/S0012-821X\(99\)00219-8](https://doi.org/10.1016/S0012-821X(99)00219-8).
- Sakaguchi, A., 1999b, Thermal structure and paleo-heat flow in the Shimanto accretionary prism, Southwest Japan: *The Island Arc*, v. 8, p. 359–372, <https://doi.org/10.1046/j.1440-1738.1999.00246.x>.
- Salot, P., Dal Piaz, G.V., and Frey, M., 1980, Métamorphisme de haute pression dans les Alpes franco-italo-suisse: *Géologie Alpine*, v. 56, p. 203–235.
- Scambelluri, M., and Philippot, P., 2004, Volatile and mobile element recycling during subduction of the oceanic lithosphere: Insights from metasediments and serpentinites of the Alps: *Periodico di Mineralogia*, v. 73, p. 221–233.
- Scambelluri, M., Picardo, G.B., Philippot, P., Robbiano, A., and Negretti, L., 1997, High salinity fluid inclusions formed from recycled seawater in deeply subducted alpine serpentinite: *Earth and Planetary Science Letters*, v. 148, p. 485–499, [https://doi.org/10.1016/S0012-821X\(97\)00043-5](https://doi.org/10.1016/S0012-821X(97)00043-5).
- Scambelluri, M., Fiebig, J., Malaspina, N., Muntener, O., and Pettke, T., 2004, Serpentine subduction: Implications for fluid processes and trace-element recycling: *International Geology Review*, v. 46, p. 595–613, <https://doi.org/10.2747/0020-6814.46.7.595>.
- Shi, Y., and Wang, C.-Y., 1985, High pore pressure generation in sediments in front of the Barbados ridge complex: *Geophysical Research Letters*, v. 12, p. 773–776, <https://doi.org/10.1029/GL012i011p00773>.
- Shiple, T.H., Stoffa, P.L., and Dean, D.F., 1990, Underthrust sediments, fluid migration paths, and mud volcanoes associated with the accretionary wedge off Costa Rica: Middle America Trench: *Journal of Geophysical Research*, v. 95, p. 8743–8752, <https://doi.org/10.1029/JB095iB06p08743>.
- Sibson, R.H., 1994, Crustal stress, faulting and fluid flow: Geological Society of London, Special Publications, v. 78, p. 69–84, <https://doi.org/10.1144/GSL.SP.1994.078.01.07>.
- Sibson, R.H., Robert, F., and Poulsen, K.H., 1988, High-angle reverse faults, fluid-pressure cycling, and mesothermal gold-quartz deposits: *Geology*, v. 16, p. 551–555, [https://doi.org/10.1130/0091-7613\(1988\)016<0551:HARFFP>2.3.CO;2](https://doi.org/10.1130/0091-7613(1988)016<0551:HARFFP>2.3.CO;2).
- Stampfli, G.M., and Marchant, R.H., 1997, Geodynamic evolution of the Tethyan margins of the Western Alps, in Pfiffner, O.A., et al., eds., *Deep Structure of the Swiss Alps: Results of NRP-20*: Basel, Birkhauser, p. 223–239.
- Sterner, S.M., and Bodnar, R.J., 1989, Synthetic fluid inclusions—VII. Re-equilibration of fluid inclusions in quartz during laboratory-simulated metamorphic burial and uplift: *Journal of Metamorphic Geology*, v. 7, p. 243–260, <https://doi.org/10.1111/j.1525-1314.1989.tb00587.x>.
- Sterner, S.M., Hall, D.L., and Keppler, H., 1995, Compositional re-equilibration of fluid inclusions in quartz: *Contributions to Mineralogy and Petrology*, v. 119, p. 1–15, <https://doi.org/10.1007/BF00310713>.
- Taira, A., Tashiro, M., Okamura, M., and Katto, J., 1980, The geology of the Shimanto Belt in Kochi prefecture, Shikoku, in Taira, A., and Tashiro, H., eds., *Geology and Paleontology of the Shimanto Belt*: Kochi, Rinyo Kosaikai Press, p. 319–389.
- Taira, A., Katto, J., Tashiro, M., Okamura, M., and Kodama, K., 1988, The Shimanto Belt in Shikoku, Japan—Evolution of Cretaceous to Miocene accretionary prism: *Modern Geology*, v. 12, p. 5–46.
- Tobin, H.J., and Saffer, D.M., 2009, Elevated fluid pressure and extreme mechanical weakness of a plate boundary thrust, Nankai Trough subduction zone: *Geology*, v. 37, p. 679–682, <https://doi.org/10.1130/G25752A.1>.
- Toriumi, M., and Teruya, J., 1988, Tectono-metamorphism of the Shimanto Belt: *Modern Geology*, v. 12, p. 303–324.
- Tsuji, T., Kimura, G., Okamoto, S., Kono, F., Mochinaga, H., Saeki, T., and Tokuyama, H., 2006, Modern and ancient seismogenic out-of-sequence thrusts in the Nankai accretionary prism: Comparison of laboratory-derived physical properties and seismic reflection data: *Geophysical Research Letters*, v. 33, L18309, <https://doi.org/10.1029/2006GL027025>.

- Underwood, M., Byrne, T., Hibbard, J.P., and DiTullio, L., 1993, A comparison among organic and inorganic indicators of diagenesis and low-temperature metamorphism, Tertiary Shimanto Belt, Shikoku, Japan, *in* Underwood, M., ed., *Thermal Evolution of the Tertiary Shimanto Belt, Southwest Japan: An Example of Ridge-Trench Interaction*: Geological Society of America Special Paper 273, p. 45–62, <https://doi.org/10.1130/SPE273-p45>.
- van Keken, P.E., Hacker, B.R., Syracuse, E.M., and Abers, G.A., 2011, Subduction factory: 4. Depth-dependent flux of H<sub>2</sub>O from subducting slabs worldwide: *Journal of Geophysical Research*, v. 116, B01401, <https://doi.org/10.1029/2010JB007922>.
- Vannucchi, P., Remitti, F., Bettelli, G., Boschi, C., and Dallai, L., 2010, Fluid history related to the Early Eocene–Middle Miocene convergent system of the Northern Apennines (Italy): Constraints from structural and isotopic studies: *Journal of Geophysical Research*, v. 115, B05405, <https://doi.org/10.1029/2009JB006590>.
- Vityk, M.O., and Bodnar, R.J., 1995a, Do fluid inclusions in high-grade metamorphic terranes preserve peak metamorphic density during retrograde decompression?: *The American Mineralogist*, v. 80, p. 641–644.
- Vityk, M.O., and Bodnar, R.J., 1995b, Textural evolution of synthetic fluid inclusions in quartz during reequilibration, with applications to tectonic reconstruction: *Contributions to Mineralogy and Petrology*, v. 121, p. 309–323, <https://doi.org/10.1007/BF02688246>.
- Vityk, M.O., Bodnar, R.J., and Doukhan, J.C., 2000, Synthetic fluid inclusions. XV. TEM investigation of plastic flow associated with reequilibration of fluid inclusions in natural quartz: *Contributions to Mineralogy and Petrology*, v. 139, p. 285–297, <https://doi.org/10.1007/s004100000142>.
- Vrolijk, P., 1987a, Tectonically-driven fluid flow in the Kodiak accretionary complex, Alaska: *Geology*, v. 15, no. 5, p. 466–469, [https://doi.org/10.1130/0091-7613\(1987\)15<466:TDFFIT>2.0.CO;2](https://doi.org/10.1130/0091-7613(1987)15<466:TDFFIT>2.0.CO;2).
- Vrolijk, P., 1987b, Paleohydrogeology and fluid evolution of the Kodiak accretionary complex, Alaska [Ph.D. thesis]: Santa Cruz, University of California, 232 p.
- Vrolijk, P., Myers, G. and Moore, J.C., 1988, Warm fluid migration along tectonic mélanges in the Kodiak accretionary complex, Alaska: *Journal of Geophysical Research*, v. 93, p. 10,313–10,324.
- Wagner, W., and Pruss, A., 2002, The IAPWS formulation 1995 for the thermodynamic properties of ordinary water substance for general and scientific use: *Journal of Physical and Chemical Reference Data*, v. 31, p. 387–535, <https://doi.org/10.1063/1.1461829>.
- Yamaguchi, A., Cox, S.F., Kimura, G., and Okamoto, S., 2011, Dynamic changes in fluid redox state associated with episodic fault rupture along a megasplay fault in a subduction zone: *Earth and Planetary Science Letters*, v. 302, p. 369–377, <https://doi.org/10.1016/j.epsl.2010.12.029>.
- Yamaguchi, A., Ujiie, K., Nakai, S., and Kimura, G., 2012, Sources and physicochemical characteristics of fluids along a subduction-zone megathrust: A geochemical approach using syntectonic mineral veins in the Mugi mélange, Shimanto accretionary complex: *Geochemistry, Geophysics, Geosystems*, v. 13, no. 7, Q0AD24, <https://doi.org/10.1029/2012GC004137>.
- Yoshida, K., Hirajima, T., Ohsawa, S., Kobayashi, T., Mishima, T., and Sengen, Y., 2015, Geochemical features and relative B-Li-Cl compositions of deep-origin fluids trapped in high-pressure metamorphic rocks: *Lithos*, v. 226, p. 50–64, <https://doi.org/10.1016/j.lithos.2015.03.002>.